Atmos. Chem. Phys., 13, 6117–6137, 2013
www.atmos-chem-phys.net/13/6117/2013/
doi:10.5194/acp-13-6117-2013
© Author(s) 2013. CC Attribution 3.0 License.

Atmospheric Chemistry and Physics
Open Access

Impact of a future H_2-based road transportation sector on the composition and chemistry of the atmosphere – Part 1: Tropospheric composition and air quality

D. Wang[1], **W. Jia**[1], **S. C. Olsen**[1], **D. J. Wuebbles**[1], **M. K. Dubey**[2], **and A. A. Rockett**[3]

[1]Department of Atmospheric Sciences, University of Illinois at Urbana-Champaign, Urbana, IL, USA
[2]Earth Systems Observations, Los Alamos National Lab, Los Alamos, NM, USA
[3]Department of Materials Science and Engineering, University of Illinois at Urbana-Champaign, Urbana, IL, USA

Correspondence to: D. J. Wuebbles (wuebbles@atmos.uiuc.edu)

Received: 16 March 2012 – Published in Atmos. Chem. Phys. Discuss.: 6 August 2012
Revised: 3 June 2013 – Accepted: 3 June 2013 – Published: 1 July 2013

Abstract. Vehicles burning fossil fuel emit a number of substances that change the composition and chemistry of the atmosphere, and contribute to global air and water pollution and climate change. For example, nitrogen oxides and volatile organic compounds (VOCs) emitted as byproducts of fossil fuel combustion are key precursors to ground-level ozone and aerosol formation. In addition, on-road vehicles are major CO_2 emitters. In order to tackle these problems, molecular hydrogen (H_2) has been proposed as an energy carrier to substitute for fossil fuels in the future. However, before implementing any such strategy it is crucial to evaluate its potential impacts on air quality and climate. Here, we evaluate the impact of a future (2050) H_2-based road transportation sector on tropospheric chemistry and air quality for several possible growth and technology adoption scenarios. The growth scenarios are based on the high and low emissions Intergovernmental Panel on Climate Change Special Report on Emissions Scenarios, A1FI and B1, respectively. The technological adoption scenarios include H_2 fuel cell and H_2 internal combustion engine options. The impacts are evaluated with the Community Atmospheric Model Chemistry global chemistry transport model (CAM-Chem). Higher resolution simulations focusing on the contiguous United States are also carried out with the Community Multiscale Air Quality Modeling System (CMAQ) regional chemistry transport model. For all scenarios future air quality improves with the adoption of a H_2-based road transportation sector; however, the magnitude and type of improvement depend on the scenario. Model results show that the adoption of H_2 fuel cells would decrease tropospheric burdens of ozone (7 %), CO (14 %), NO_x (16 %), soot (17 %), sulfate aerosol (4 %), and ammonium nitrate aerosol (12 %) in the A1FI scenario, and would decrease those of ozone (5 %), CO (4 %), NO_x (11 %), soot (7 %), sulfate aerosol (4 %), and ammonium nitrate aerosol (9 %) in the B1 scenario. The adoption of H_2 internal combustion engines would decrease tropospheric burdens of ozone (1 %), CO (18 %), soot (17 %), and sulfate aerosol (3 %) in the A1FI scenario, and would decrease those of ozone (1 %), CO (7 %), soot (7 %), and sulfate aerosol (3 %) in the B1 scenario. In the future, people residing in the contiguous United States could expect to experience significantly fewer days of elevated levels of pollution if a H_2 fuel cell road transportation sector were to be adopted. Health benefits of transitioning to a H_2 economy for citizens in developing nations, like China and India, will be much more dramatic, particularly in megacities with severe, intensifying air-quality problems.

1 Introduction

Fossil fuel combustion in on-road vehicles emits a number of pollutants directly into the surrounding air. The exhaust air contains nitrogen oxides ($NO_x = NO + NO_2$), carbon monoxide (CO), volatile organic compounds (VOCs), and particulate matter. These byproducts can have adverse impacts on human health. For example, sustained high levels of NO_2 have an adverse impact on the respiratory system

Published by Copernicus Publications on behalf of the European Geosciences Union.

as elevated CO concentrations degrade the ability of blood to transport oxygen (e.g., WHO/Europe, 2003). In addition, NO_x, CO and VOCs are precursors to the formation of ground-level ozone (O_3), which adversely impacts human health and ecosystems in a number of ways. Particulate matter, which raises concern of physiological hazard, is either directly released in the form of soot (black carbon) or formed indirectly from gaseous pollutants through a series of photochemical and physical processes (sulfate and secondary organics). In the United States, on-road vehicles rank first in NO_x and CO emissions and second in VOCs emissions among all source sectors (US EPA, 2009). In the future the on-road vehicle fleet is expected to become an increasingly more important contributor to ambient air pollution.

Molecular hydrogen (H_2) has been proposed as an alternative energy carrier for on-road vehicles since it has higher energy efficiency and much cleaner oxidation products. Since H_2 fuel cells emit only water vapor (H_2O), tailpipe emissions of NO_x, CO, VOCs, and soot associated with fossil fuel combustion are eliminated. In addition to being oxidized in fuel cells, H_2 can also be burned in internal combustion engines. In this paper, the impact of both the H2 fuel cell and internal combustion engine options will be investigated. Vehicles powered by H_2 internal combustion engines emit no CO, VOCs, or soot but do emit NO_x. Additionally, in each of these scenarios some H_2 is emitted due to leakage during its production, distribution, and storage. Given the reductions in tailpipe pollutant emissions, it is reasonably foreseeable that transitioning the world's road traffic from fossil fuel powered vehicles to H_2 powered vehicles could substantially improve air quality and climate, provided that the H_2 is produced by non-polluting methods, e.g., wind, solar, nuclear power, hydroelectricity or, promisingly, photocatalytic and photoelectrochemical dissociation of water (Abe, 2010) and microbial reverse-electrodialysis electrolysis cells (Kim and Logan, 2011). Even if H_2 is generated conventionally from fossil fuel, it would be easier to control the pollutant emissions from H_2 production since they would be emitted from relatively few locations and the produced CO_2 could be sequestered. This paper aims at quantitative evaluation of the potential environmental impacts of such a transition.

Tropospheric H_2 concentrations are currently around 530 ppbv (Novelli et al., 1999), making it second to CH_4 as the most abundant oxidizable gas in the atmosphere (Constant et al., 2009). The primary sources of H_2 are fossil fuel and biofuel combustion, biomass burning, ocean emissions, and photolysis of formaldehyde. Bottom-up inventories estimate its source as $\sim 75\,TgH_2\,yr^{-1}$ (Ehhalt and Rohrer, 2009). Its largest sink ($\sim 80\,\%$) is microbial uptake in soils, with oxidation by OH in the atmosphere making up the remainder of its loss (Constant et al., 2009). Its uptake by microbes in soil, despite its importance, is not well understood and is subject to large uncertainties. Observations show a correlation between the H_2 and CO deposition velocities (Conrad and Seiler, 1985; Liebl and Seiler, 1976; Yonemura et al., 1999, 2000). Recently there have been attempts to examine microbial H_2 uptake by different soil types under a variety of conditions (e.g., Smith-Downey et al., 2008; Constant et al., 2008). It is known that the H_2 uptake depends on soil moisture and temperature, among a number of factors. However, there still remains relatively large uncertainty in variation among ecosystems, the controlling factors, and how to map these to global ecosystems.

H_2's total atmospheric lifetime is estimated to be 1 to 2 yr (Constant et al., 2009; Ehhalt and Rohrer, 2009; Novelli et al., 1999; Price et al., 2007) and its lifetime with respect to OH loss is ~ 8 yr (Ehhalt and Rohrer, 2009). The latitudinal gradient of H_2 concentrations is unique from many other trace gases, with $\sim 3\,\%$ higher average concentrations in the Southern Hemisphere (SH) than in the Northern Hemisphere (NH). This is thought to be due to the greater soil microbial uptake over land in the NH (Ehhalt and Rohrer, 2009). Since there are no clear long-term trends (Constant et al., 2009; Ehhalt and Rohrer, 2009), a conversion to a H_2-based road transportation sector could elevate atmospheric H_2 concentrations to values not previously experienced.

Initial studies on the environmental impacts of a H_2 economy have focused mainly on the possible adverse effects of increased H_2 on stratospheric ozone. Using a two-dimensional model, Tromp et al. (2003) found that in an assumed world with a H_2-based energy source with a perhaps unrealistically large H_2 leakage rate ($\sim 12\,\%$), the surface H_2 concentration of 2.3 ppmv would lead to 3–8 % polar spring stratospheric ozone loss due to a decrease in lower stratosphere temperature. Later studies found a much smaller impact (less than 1 %) on stratospheric ozone (Warwick et al., 2004), and instead focused on the relatively large improvements in tropospheric air quality due to the reduction in ozone precursor emissions.

A 3-D modeling study by Schultz et al. (2003) suggested a H_2 fuel cell road traffic fleet in ca. 2000 would reduce human emissions of NO_x and CO by half, resulting in 3 %, 6 %, 5 % and 29 % decrease in tropospheric CO, OH, O_3 and NO_x, respectively; tropospheric H_2 burden would increase by 28 %, assuming a 3 % leakage rate. Warwick et al. (2004) reported an estimated 2.2 % decrease in tropospheric O_3 in a H_2 economy based on a 2-D modeling study. Jacobson et al. (2005) compared the environmental impact of a 1999 hydrogen on-road vehicle fleet in the US by means of steam reforming of natural gas, wind electrolysis, and coal gasification; they found the wind and natural gas options to have the best desired environmental improvement.

Although H_2 is not a direct greenhouse gas and its utilization could provide opportunities to offset CO_2 emissions, concern has arisen due to its indirect greenhouse potential (e.g., Prather, 2003). Through its reaction with OH, increases in H_2 concentration could decrease the oxidizing capacity of the troposphere and hence increase the CH_4 lifetime. CH_4 is an ozone precursor and a long-lived greenhouse gas that is 25 times more powerful than CO_2 in terms of integrated radiative forcing over a 100 yr time horizon. Currently its radiative forcing is second only to that of CO_2 (IPCC, 2007). Derwent et al. (2006) estimated that the climate impact of 1 % leakage of H_2 is 0.6 % of that of the replaced CO_2.

The impact of the reductions in ozone precursor emissions may be significant on the oxidizing capacity of the troposphere as well. Taking this effect into account, the decrease in tropospheric OH abundance ranges from 0 % to 12 %, and the increase in CH_4 lifetime ranges from 0 % to 26 %, depending on the specific scenario assumed (Jacobson, 2008; Schultz et al., 2003; Warwick et al., 2004).

All of these previous studies were based on the then current (ca. 2000) background atmosphere, focused on a conversion of the then current infrastructure, and assumed an immediate transition to hydrogen technology. The transition to hydrogen-based energy delivery will, in real-world practice, require the development of a massive industrial H_2 production capacity and substantial changes to the energy delivery infrastructure, and there are still a number of technological barriers yet to overcome. Considering the time needed to make the current infrastructure H_2-compatible, we evaluate the impacts of a transition occurring in the future that allows a reasonable amount of time for the infrastructure changes to occur. Thus, we assume that in the coming decades road transportation will transform to H_2 powered such that the transition will be complete by 2050. That is, all on-road vehicles operating in 2050 will be powered by H_2.

In this study we assess the impact on the composition and chemistry of the troposphere in 2050 due to 100 % conversion of the road transportation system from fossil fuel to H_2. To accomplish this we develop 2050 emissions scenarios for continued use of fossil fuel and for a H_2-based transportation sector. The emissions scenarios encompass several possible growth and technology adoption paths. The growth scenarios are based on the high and low emitting Intergovernmental Panel on Climate Change (IPCC) Special Report on Emissions Scenarios (SRES), A1FI and B1, respectively. The technological adoption scenarios include H_2 fuel cell and H_2 internal combustion engine options. The impacts of these emissions are evaluated using the Community Atmosphere Model with Chemistry (CAM-Chem) three-dimensional global climate-chemistry model. In addition, we evaluate the air quality impact over the contiguous United States using the Community Multiscale Air Quality Modeling System (CMAQ) regional air quality model. The development of the emissions scenarios is discussed in Sect. 2, the models are described in Sect. 3, and the results are presented in Sect. 4.

2 Emission scenarios

Emissions of a given species are often estimated based on emissions factors, which relate the emissions of a given pollutant to an activity and to the level of the activity. Thus, projections of future emissions are based on projections of the change in the activity level and the changes in the emissions factors. Commonly, the activity factors include population, energy usage, and GDP. Since there are large uncertainties in projecting the change in each of these activities over time, there are also relatively large uncertainties in the emissions estimates based on them. To bracket the possible evolution pathways of the future emissions, we develop scenarios based on the highest (A1FI) and lowest (B1) IPCC SRES emissions scenarios (IPCC, 2000). In the A1FI scenario, the world is assumed to evolve with rapid economic growth and rely intensively on fossil fuel; in the B1 scenario, the world's economic structures are projected to become more service and information intensive. For each of these two IPCC growth scenarios (A1FI and B1), three emission scenarios with different technologies were developed. (1) In this future baseline (BL) scenario, the reference scenario for 2050, fossil fuel powered vehicles remain the dominant mode of road transportation. (2) In the H_2 fuel cell (H_2-FC) scenario, energy demands of the road transportation sector are met by H_2 fuel cell technology. In H_2-FC scenario, H_2 emissions due to leakage as well as reductions in combustion-related emissions of H_2, NO_x, VOCs, CO, SO_2, and soot are included. (3) In the H_2 internal combustion engine H_2-ICE scenario, energy demands of the road transportation sector are met by H_2 using internal combustion technology. In H_2-ICE scenario, H_2 emissions due to leakage as well as reductions in combustion-related emissions of H_2, VOCs, CO, SO_2 and soot are included, as in H_2-FC scenario; however, unlike H_2-FC scenario, there are no reductions in NO_x emissions because NO_x is still a byproduct of internal combustion process regardless of the type of fuel. For each IPCC scenario, an additional scenario, baseline + H_2 (BL + H_2), was developed. In this additional scenario, H_2 emissions leakage into the atmosphere was included but all other emissions remain as described above. This H_2 emissions leakage scenario, though not realistic, is designed as a sensitivity study in order to evaluate and compare the impact of H_2 emission alone versus the impact of the reduction in ozone precursors emissions on tropospheric composition and chemistry.

The future baseline (BL) emissions are calculated by scaling the current fossil fuel combustion emissions by regionally dependent growth scale factors from the applicable IPCC scenario. The included species are NO_x, CO, SO_2 and several NMVOCs (non-methane VOCs), namely, CH_2O, CH_3OH, CH_3CHO, C_2H_4, C_2H_6, C_2H_5OH, C_3H_6, C_3H_8, CH_3COCH_3 (acetone), C_4H_8O (methyl ethyl ketone), C_4H_{10}, C_5H_8 (isoprene), $C_{10}H_{16}$, BIGALK (lumped species for alkanes with four or more carbon atoms), BIGENE (lumped species for alkenes with four or more carbon atoms), and TOLUENE (lumped species for aromatic compounds). Emissions of these species are prepared from the Precursors of Ozone and their Effects in the Troposphere (POET) emissions dataset, which is based on version 3 of the Emission

Database for Global Atmospheric Research (EDGAR) inventory (Olivier et al., 2003; Granier et al., 2005). This dataset represents the period between 1990 and 2000. Soot emissions are from Bond et al. (2004), derived from 1996 fuel-use data.

To estimate H_2 emissions from fossil fuel combustion, which are not included in the IPCC scenarios or POET, we use a $H_2:CO$ mass emission factor of 0.03 and the corresponding CO emissions. There is a relatively large uncertainty in the $H_2:CO$ mass emission ratio from fossil fuel use, including automobile traffic. Estimates range from ~ 0.01 (Simmonds et al., 2000) to ~ 0.07 (Seiler and Zankl, 1975). Other estimates are 0.025–0.032 (Barnes et al., 2003) and 0.026–0.043 (Vollmer et al., 2007). For this study we choose a mid-value of 0.03 and assume it remains constant over time.

In the scenarios involving H_2 technologies, we estimate H_2 emissions from leakage using a top-down approach based on a H_2 leakage rate and the amount of H_2 needed to meet the projected transportation energy demands in 2050. H_2 demand for road transportation is calculated assuming both the H_2-FC and the H_2-ICE vehicles would have comparable efficiencies as fossil fuel vehicles in 2050 due to technology improvement, such that H_2-powered vehicles will consume the same amount of energy as that of the year 2050 "business-as-usual" fleet in the IPCC A1FI and B1 baseline scenarios. Total H_2 demand is then calculated assuming a 120 MJ kg^{-1} energy density of hydrogen. Current estimates of the H_2 leakage rate are in the 1 % to 4 % range (e.g., Schultz et al., 2003; Colella et al., 2005). Here we assume a H_2 leakage rate of 2.5 %. To date, confidence in the current knowledge of H_2 leakage rates is low and we are not aware of any real-world measurements of the leakage rates. Our estimate is in line with estimated leakage from natural gas production, supply and delivery systems. Knowledge of actual leakage rates, their dependence on technological sophistication, and how they will change in the future is one of the key uncertainties in estimating future hydrogen leakage emissions. The total H_2 emissions for a given scenario are then obtained by replacing the road transportation H_2 emissions from fossil fuel combustion with the H_2 leakage emissions for the H_2 scenarios. H_2 leakage emissions are distributed according to current CO_2 road transportation emissions from the EDGAR emissions inventory, with higher H_2 leakage emissions over more densely populated areas such as the eastern United States, Western Europe, parts of India and eastern China.

For all of the H_2 scenarios (BL + H_2, H_2-FC, and H_2-ICE), H_2 leakage emissions are included. In the H_2-FC scenarios, the road transportation emissions of H_2, CO, NO_x, NMVOCs, SO_2, and soot are removed from the total baseline (BL) emissions. In the H_2-ICE scenarios, the emissions of the same species as in the H_2-FC scenarios are reduced except for NO_x, which is still emitted with the ICE technology option.

Biomass burning emissions are from the Global Fire Emissions Database version 2 (GFED-v2) (van der Werf et al., 2006) and are assumed to remain at their 2000 levels as are emissions from other sources, e.g., ocean and biogenic emissions.

Annual global emissions of key species of current (2000) and 2050 (baseline and H_2 scenarios) are summarized in Fig. 1. Global emissions increase relative to 2000 in the 2050 A1FI baseline (A1FI BL) scenario for H_2 (42 %), CO (35 %), NMVOCs (28 %), NO_x (115 %), SO_2 (10 %), and soot (67 %). In the 2050 B1 baseline (B1 BL) scenario, global emissions decrease from 2000 for H_2 (19 %), CO (10 %), NMVOCs (6 %), SO_2 (7 %), and soot (12 %); NO_x emissions increase by 5 %.

In the A1FI scenarios with a H_2 road transportation sector, global H_2 emissions increase by 81 % relative to the 2050 A1FI baseline (A1FI BL) scenario, or increase by 157 % from the 2000 emissions. Meanwhile, global emissions in the 2050 H_2-FC and H_2-ICE scenarios decrease for CO (25 %), NMVOCs (14 %), NO_x (29 % in H_2-FC; 0 % in H_2-ICE), SO_2 (3 %) and soot (17 %), compared to the 2050 A1FI baseline (A1FI BL) scenario. Compared to the 2000 emissions, in a 2050 A1FI world with a H_2 road transportation sector, emissions increase to a lesser extent than in the A1FI baseline scenario: CO (1.6 %), NMVOCs (10 %), NO_x (53 % in H_2-FC), SO_2 (7 %) and soot (39 %),.

In the B1 scenarios with a H_2 road transportation sector, global H_2 emissions increase by 64 % relative to the 2050 B1 baseline (B1 BL) scenario, or increase by 33 % from the 2000 emissions. Concurrently, global emissions in the 2050 H_2-FC and H_2-ICE scenarios decrease for CO (10 %), NMVOCs (8 %), NO_x (24 % in H_2-FC; 0 % in H_2-ICE), SO_2 (3 %) and soot (8 %), compared to the 2050 B1 baseline (B1 BL) scenario. If compared with the 2000 emissions, in a 2050 B1 world with a H_2 road transportation sector, emissions decrease to a greater extent than in the B1 baseline scenario: CO (19 %), NMVOCs (13 %), NO_x (20 % in H_2-FC), SO_2 (10 %) and soot (19 %).

These emissions are input to the model as monthly varying maps at the model resolution.

3 Model description

For the global model simulations in this study we use the Community Atmosphere Model with Chemistry (CAM-Chem) three-dimensional climate-chemistry model (Lamarque et al., 2005; Pfister et al., 2008). CAM-Chem's chemistry module is based on the chemical component of the Model for OZone And Related chemical Tracers (MOZART). MOZART was described and extensively evaluated by Horowitz et al. (2003), and has been employed in a number of studies (e.g., Huang et al., 2008; Lin et al., 2008a, b; Tie et al., 2005). It contains a comprehensive tropospheric gas phase and aerosol chemical mechanism and includes 119 species and 300 reactions. CAM-Chem uses a bulk aerosol method and includes organic carbon, black carbon, sulfate, and ammonium nitrate aerosols. Based on the

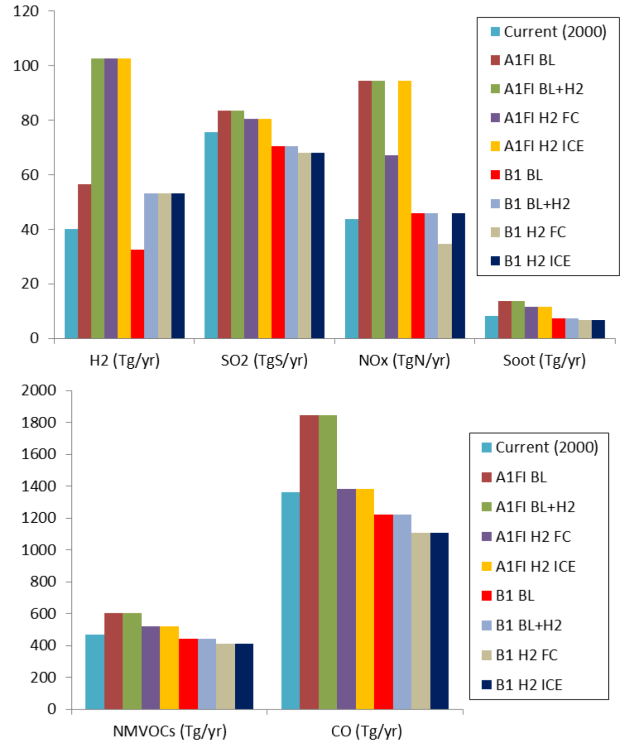

Fig. 1. Global annual emissions of H_2, SO_2, NO_x, soot, NMVOCs and CO for the current (year 2000), and the 2050 A1FI and B1 scenarios: baseline (BL), baseline + H_2 (BL + H_2), H_2 fuel cell (H_2-FC), and H_2 internal combustion engine (H_2-ICE) .

observed correlation between H_2 and CO deposition velocities (Conrad and Seiler, 1985; Liebl and Seiler, 1976; Yonemura et al., 1999, 2000), we adopt a H_2 deposition velocity equal to twice the CO deposition velocity.

For this study, the global atmosphere is divided into grids with a horizontal resolution of 1.9° latitude by 2.5° longitude, and 26 vertical layers extending from the surface to 3-millibar level (∼ 40 km altitude). The meteorology is prescribed by climate model output data from Community Climate System Model (CCSM), which corresponds to the climate state of the mid-1990s. We choose to use this meteorology since our focus in this study is on air quality and photochemistry-influenced impacts due to changes in emissions. Previous studies (e.g., Lin et al., 2008a; Wu et al., 2008) have shown that future climate changes will likely have less effect on air quality than the future changes in emissions. The model is integrated with a time step of 30 min. After completion of one year's calculation, the meteorology field is repeated for the next year. This method allows the impact of changes in emissions to be investigated excluding the possible influences of changes in meteorology. The 2050 monthly mean lower boundary CH_4 concentrations are scaled from the 2000 value (annual mean 1776 ppbv) to the concentrations projected by IPCC (2001) for 2050, 2668 ppbv for the A1FI scenario and 1881 ppbv for the B1 scenario. The model is run for eight years and has reached steady state, that is, year-to-year relative difference of key species is less than 1 %. Our analysis is based on results from the last year of simulation.

In order to assess the regional air quality impacts of a H_2-based road transportation sector on the contiguous United States with finer resolution, we use the Community Multiscale Air Quality Modeling System (CMAQ) version 4.6. The CMAQ model was initially released to the public by the United States Environmental Protection Agency (US EPA) in 1998 and has undergone many revisions and improvements since (e.g., Appel et al., 2007, 2008). The CMAQ modeling system was designed to approach air quality as a whole by including state-of-the-science capabilities for modeling multiple air quality issues, including tropospheric ozone, fine particles, toxics, acid deposition, and visibility degradation. For this study the CMAQ horizontal resolution is 30 km by 30 km with 22 vertical layers from the surface to 13 km, with a relatively finer resolution in the boundary layer with 5 layers in the first km. The meteorological data driving CMAQ is from a climate version of the MM5 model (CMM5; e.g., Liang et al., 2001) for the year 1995. For this study CMAQ uses the Carbon Bond 5 gas phase photochemistry package (Luecken, et al., 2008; Sarwar, et al., 2008) with 56 species and 156 reactions. The aerosol chemistry package is coupled to the gas phase chemistry package and contains 34 transported aerosol modes. The aerosol package represents the particle size distribution as the superposition of three lognormal modes. The processes of coagulation, particle growth by the addition of new mass, and particle formation are included. Time stepping is done utilizing an analytical solution to the differential equations for the conservation of number and species mass conservation. The simulation was carried out with a 12 min dynamical time step and the chemistry package using a 2.5 min sub-time step. Detailed descriptions of the mechanisms, algorithms, and implementation are available in the CMAQ scientific documentation (Byun and Schere, 2006). Boundary conditions for the CMAQ model simulations are taken from the corresponding global tropospheric model simulations. The CMAQ simulations are performed for the BL, H_2-FC, and H_2-ICE scenarios for each IPCC scenario.

4 Model results and discussion

Overall, H_2 concentrations increase substantially in all H_2 scenarios and air quality improves with the adoption of a H_2-based road transportation sector; however, the magnitude and quality of improvement depends on the scenario. While the changes in H_2 concentrations are sensitive to uncertainties in the assumed H_2 leakage rate of 2.5 %, the changes in air quality, e.g., O_3, are driven by changes in ozone precursor emissions that are not related to the assumed H_2 leakage rate. Each relevant species is discussed in detail below.

Table 1. Tropospheric mean mixing ratios or concentrations for the 2000 atmosphere, the 2050 A1FI baseline scenario and percent changes for the baseline + H_2 (BL+H_2), hydrogen fuel cell (H_2-FC), and hydrogen internal combustion engine (H_2-ICE) scenarios from the 2050 A1FI baseline scenario simulated by the CAM-Chem model.

	2000	2050 Baseline	BL+H_2	H_2-FC	H_2-ICE
H_2	626 ppbv	839 ppbv	41 %	40 %	38 %
O_3	37 ppbv	44 ppbv	0 %	−7 %	−1 %
OH	9.7×10^5 molecules cm^{-3}	9.1×10^5 molecules cm^{-3}	−2 %	−4 %	7 %
CO	97 ppbv	133 ppbv	1 %	−14 %	−18 %
NO_x	60 pptv	100 pptv	0 %	−16 %	10 %
soot	0.025 µgC m^{-3}	0.025 µgC m^{-3}	0 %	−17 %	−17 %
SO_4	0.30 µgSO_4 m^{-3}	0.34 µgSO_4 m^{-3}	0 %	−4 %	−3 %
NH_4NO_3	0.010 µg m^{-3}	0.014 µg m^{-3}	0 %	−12 %	3 %

4.1 Molecular hydrogen

In all of the scenarios examined in this study, average tropospheric H_2 concentrations are greater in 2050 than they are in 2000. In the A1FI baseline scenario the annual average global mean concentration is 839 ppbv (Table 1). The H_2 lifetime in the A1FI 2050 baseline scenario is essentially unchanged from its value of 2.5 yr in the year 2000 simulated atmosphere. In this scenario the NH emissions are strong enough to offset the stronger soil sink in this hemisphere, leading to a reverse in the inter-hemispheric gradient, i.e., higher NH mean H_2 concentration (∼ 850 ppbv) than SH (∼ 830 ppbv). Annual-mean ground-level H_2 mixing ratios range from 720 ppbv to more than 1 ppmv (Fig. 2a). Higher concentrations are located in highly urbanized and/or industrialized regions such as northeastern United States, California, Western Europe, Korea, Japan and eastern China, while lower concentrations appear over mid-latitude continents of the SH. The maximum/minimum pattern reflects the forcing of the H_2 emissions from human activities and the large H_2 microbial soil sink.

In the A1FI H_2 technology scenarios (BL+H_2, H_2-FC, and H_2-ICE), global mean H_2 concentrations increase substantially from the baseline scenario by ∼ 40 %, to up to ∼ 1170 ppbv (Table 1). The H_2 lifetime in the H_2-FC scenario is the same as in the baseline simulation (2.5 yr) but decreases slightly (by ∼ 3 %) in the H_2-ICE scenario. This increase is because the H_2 leakage emissions are much greater than the replaced fossil fuel H_2 emissions in the baseline scenario. In the H_2-FC scenario the south to north H_2 inter-hemispheric gradient is even larger than in the BL scenario (Fig. 2b) since H_2 emissions increased more in the NH than in the SH due to the asymmetric intensity of road transportation activities between the hemispheres. The background surface H_2 mixing ratio increases by at least 40 % in the NH and by at least 35 % in the SH, reaching about 1.2 ppmv in the NH and 1.15 ppmv in the SH. The highest H_2 concentrations (greater than 1.6 ppmv) are in eastern China and Korea, corresponding to a greater than 75 % increase from the baseline scenario. H_2 concentrations increase by approximately 50 % in northeastern United States. The largest increase (∼ 45 %) in zonal-average H_2 concentration occurs in the boundary layer in the Northern Hemisphere mid-latitudes where road transportation activities are concentrated. The spatial distributions of the H_2 concentrations in the BL+H_2 and H_2-ICE scenarios (not shown) are nearly identical to those in the H_2-FC scenario. The geographical pattern of relative increase in surface H_2 concentrations in this scenario is similar to that calculated by Schultz et al. (2003), even though they assumed a leakage rate of 3 % and their calculation is for the year 2000 atmosphere. However, the increase in eastern Asia is comparatively larger in this study because of the projected significant economic development in this region by 2050.

In the B1 baseline scenario the average tropospheric H_2 mixing ratio is 621 ppbv (Table 2), and the annual-mean ground-level H_2 concentration is ∼ 600 ppbv (Fig. 2c). The H_2 lifetime is 2.5 yr, unchanged from the current day and A1FI baseline simulations. The inter-hemispheric gradient is of the same direction as in the current atmosphere, with higher background H_2 concentrations in the SH. Since human activities that emit H_2 are not as intensive as in the A1FI scenario, there are few regions bearing significantly higher than background value, except the northeastern United States, where H_2 concentrations are around 650 ppbv.

In the B1 H_2 scenarios (BL + H_2, H_2-FC, and H_2-ICE), the tropospheric H_2 burden increases by ∼ 20 %, corresponding to a mean tropospheric concentration of 740 ppbv. As for the A1FI simulations, the H_2 lifetime for the B1 H_2-FC simulations is unchanged at 2.5 yr while for the H_2-ICE scenario it decreases by ∼ 3 %. In the H_2-FC scenario (the other two are quite similar), surface H_2 concentrations in remote regions increase from the BL scenario by more than 20 % in the NH and by more than 15 % in the SH (Fig. 2d), leading to a slightly higher H_2 concentration in the NH, a reverse in the inter-hemispheric gradient. Maximum H_2 mixing ratios (860 ppbv) occur in eastern Asia, corresponding to a more than 40 % increase from the baseline scenario.

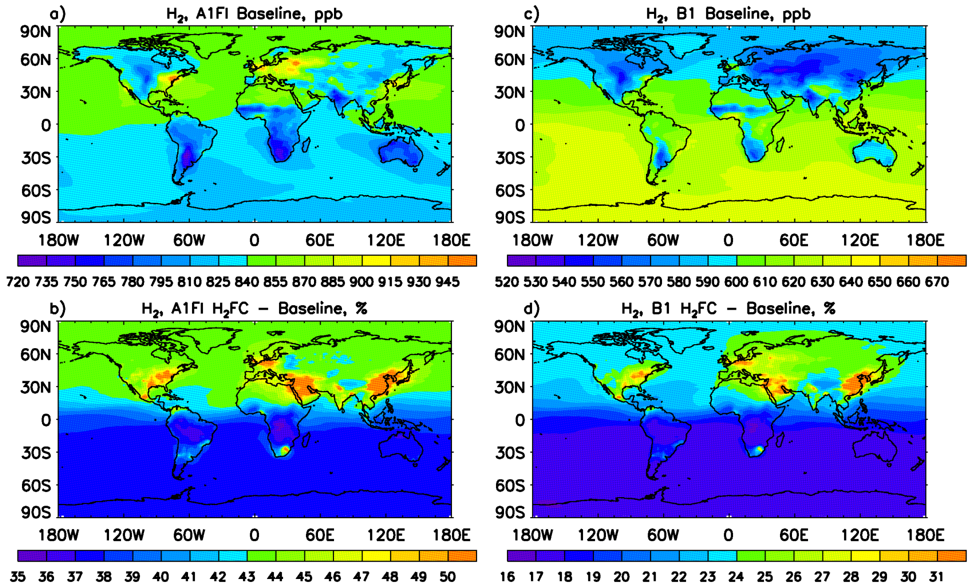

Fig. 2. CAM-Chem simulated 2050 annual-mean ground-level H_2 mixing ratios in the A1FI **(a)** and B1 **(c)** baseline scenarios and the percent differences for the A1FI **(b)** and B1 **(d)** H_2-FC scenarios. Note the different scales.

Table 2. Tropospheric mean mixing ratios or concentrations for the 2050 B1 baseline scenario and percent changes for the baseline + H_2 (BL+H_2), hydrogen fuel cell (H_2-FC), and hydrogen internal combustion engine (H_2-ICE) scenarios from the CAM-Chem model simulations.

	Baseline	BL+H_2	H_2-FC	H_2-ICE
H_2	621 ppbv	20 %	20 %	19 %
O_3	37 ppbv	0 %	−5 %	−1 %
OH	10.1×10^5 molecules cm^{-3}	−1 %	−4 %	3 %
CO	90 ppbv	0 %	−4 %	−7 %
NO_x	60 pptv	0 %	−11 %	3 %
soot	0.014 µgC m^{-3}	0 %	−7 %	−7 %
SO_4	0.33 µgSO_4 m^{-3}	0 %	−4 %	−3 %
NH_4NO_3	0.010 µg m^{-3}	0 %	−9 %	2 %

4.2 Ozone

The annual-averaged tropospheric ozone (averaged over the entire troposphere) concentration is 44 ppbv in the 2050 A1FI BL scenario, higher than the 2000 value of 39 ppbv (IPCC, 2001), due to increased precursor emissions. The summertime (June, July, and August) average surface ozone concentrations over land in the A1FI BL scenario are projected to be mostly above 40 ppbv (Fig. 3a). Summertime ozone concentrations are highest near densely populated areas, such as the eastern United States, California, the Middle East, and eastern China. In the A1FI H_2-FC scenario, surface ozone mixing ratios decrease by more than 5 % around the world, with as much as 20 % decrease in Latin America and Southeast Asia (Fig. 3b). In heavily polluted areas surface ozone mixing ratios are about 10 % lower than those in the BL scenario. However, ozone increases in some localized populated areas in eastern China, Korea, South Africa, and London, UK. In these regions ozone production is VOC-limited. The VOC-limited regime is characterized by high background NO_x concentrations with ozone production proportional to VOC concentrations but inversely proportional to NO_x concentrations (e.g., Jacob, 1999). In this case the increase in O_3 production due to the decrease in NO_x emissions wins out over the decrease in O_3 production due to the decrease in VOC emissions causing an increase in O_3 in these regions for the H_2 fuel cell scenario. While the changes in ozone extend throughout the troposphere, the largest changes occur near the surface (Fig. 4). In the A1FI H_2-FC scenario, zonally-averaged summertime ozone mixing ratios are at least 5 % lower than in the BL scenario in the lower troposphere (Fig. 4b). The maximum decrease (more than 10 %) appears in the boundary layer at the low latitudes of the NH (centered at around 15° N).

In the A1FI H_2-ICE scenario, summertime surface ozone concentrations are virtually unchanged over most of the globe (Fig. 3c). The relatively modest decreases occur over limited regions, such as England and Korea, which tend to include the highly localized regions where ozone increased in the H_2 fuel cells scenario. The zonally-averaged ozone concentrations do not change significantly except in the lower troposphere of the northern middle latitudes, where ozone decreases by as much as 5 % (Fig. 4c).

In the 2050 B1 BL scenario, the average tropospheric ozone concentration is ∼37 ppbv, slightly lower than the current value, due to slightly decreased precursor emissions

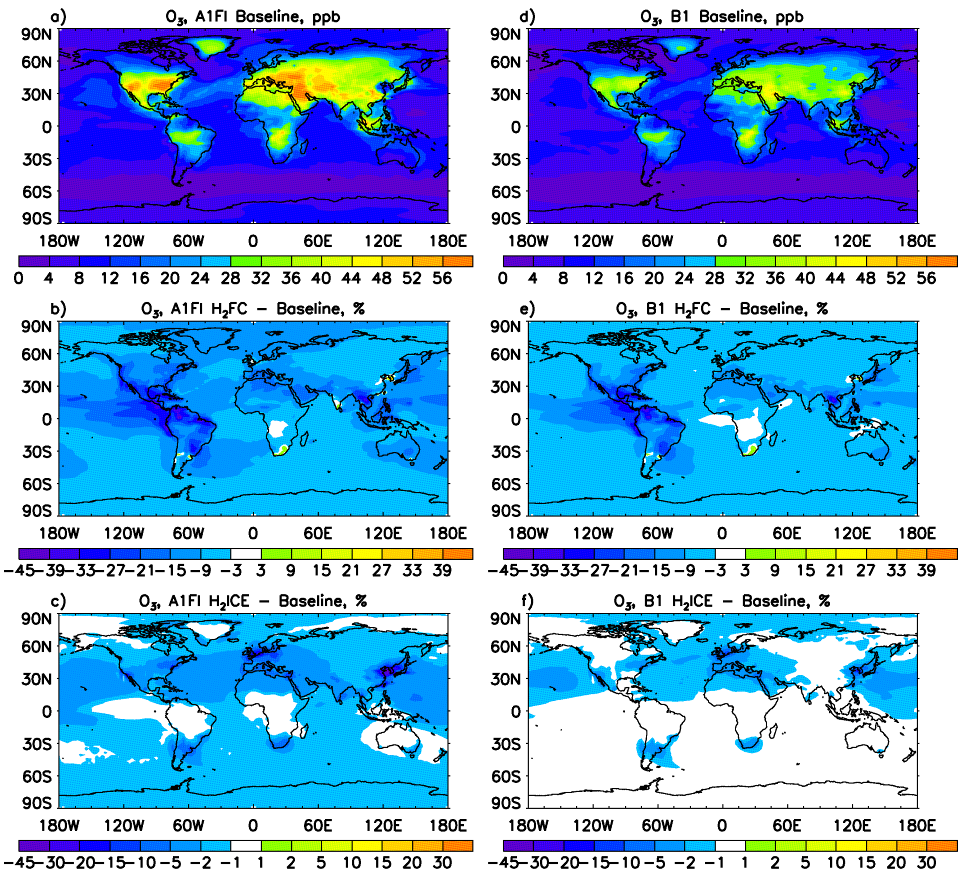

Fig. 3. CAM-Chem simulated 2050 NH summer (June, July, and August) average ground-level O_3 mixing ratios in the A1FI **(a)** and B1 **(d)** baseline scenarios and percent differences for the H_2 fuel cell (H_2-FC) and H_2 internal combustion engine (H_2-ICE) scenarios **(b, c, e, f)**. Note the different scales.

(except NO_x, which slightly increases). The distribution pattern of the summertime surface ozone concentrations over the world is similar to that for the corresponding A1FI scenarios, but the concentrations are 10–20 ppbv lower than those in the A1FI BL scenario (Figs. 3d and 4d). In the B1 H_2-FC scenario, summertime near surface ozone decreases significantly (by 10 % to 30 %) (Figs. 3e and 4e) along the coasts of the United State, making them considerably lower than current O_3 concentrations. Ozone reductions in the B1 H_2-ICE scenario are not as apparent (Figs. 3f and 4f), except in the same sensitive areas as in the A1FI H_2-ICE scenario, where relative reductions are no more than 15 %.

The simulation results of the CMAQ model over the contiguous United States is consistent with the global model results in general; however, due to its finer resolution, CMAQ is capable of capturing some of the finer features of the ozone concentrations. For example, while CAM-Chem predicts that the highest summertime ozone concentrations appear in California and the Midwest, CMAQ predicts higher maximum daily 8 h average ozone concentrations near population centers and along the US west and east coasts with a plume extending off the east coast (Fig. 5a and d). Over the southwestern United States and parts of the East Coast, daily maximum 8 h average O_3 concentrations at surface are projected to exceed the US EPA National Ambient Air Quality Standards (NAAQS) of 75 ppbv over much of the summertime for the A1FI BL scenario. In contrast, concentrations are in compliance with the NAAQS (below $\sim$56 ppbv) for the vast majority of the time for the B1 BL scenario.

Relatively large decreases in daily maximum 8 h O_3 concentrations are noted with the adoption of the H_2-FC scenarios. For both the A1FI and B1 scenarios the decreases are largest over the population centers (Fig. 5b and e). The decreases in summertime O_3 concentrations are nearly 18 ppbv for A1FI and 12 ppbv for the B1 scenario. In stark contrast to these decreases for the H_2-FC scenario, there is little decrease in daily maximum 8 h O_3 concentrations for the H_2-ICE scenario over the vast majority of the United States (Fig. 5e and f). There are some relatively small reductions over the Los Angeles and San Francisco regions of California and a few very localized spots in the Midwest but these

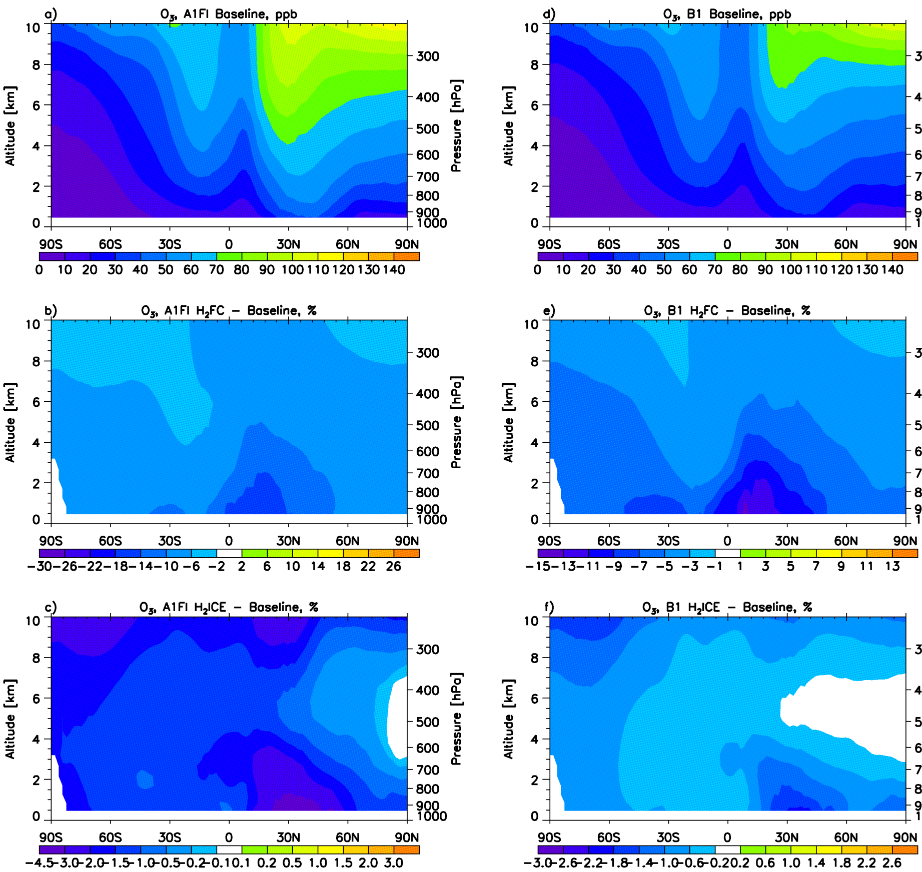

Fig. 4. CAM-Chem simulated 2050 NH summer (June, July, and August) average zonal-mean O_3 mixing ratios in the A1FI **(a)** and B1 **(d)** baseline scenarios and percent differences for the H_2 fuel cell (H_2-FC) and H_2 internal combustion engine (H_2-ICE) scenarios **(b, c, e, f)**. Note the different scales.

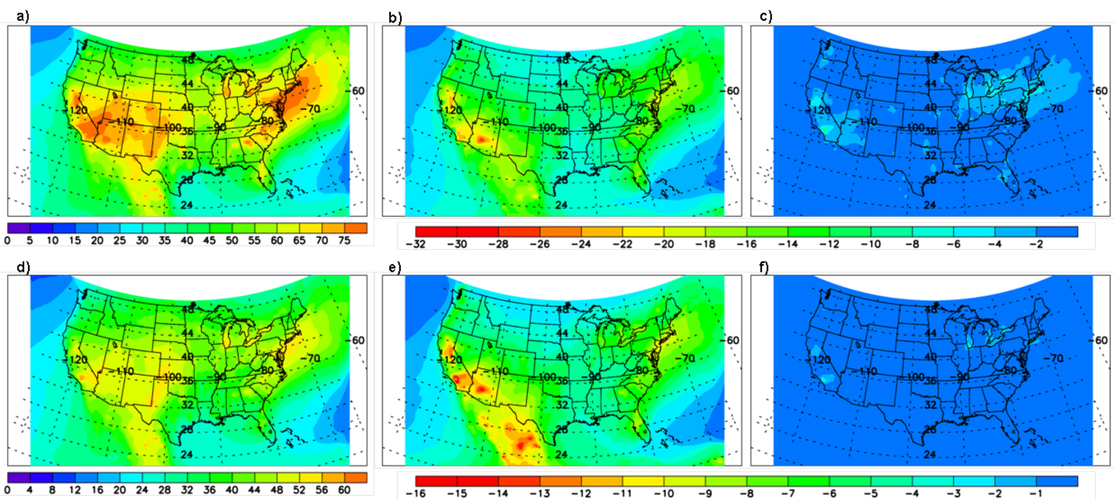

Fig. 5. July 2050 averages of the daily maximum 8 h-average O_3 concentrations simulated by CMAQ for the A1FI (top) and B1 scenarios (bottom). Each row contains the baseline scenarios (left: **a** and **d**), differences between the baseline and H_2 fuel cell (H_2-FC) scenarios (center: **b** and **e**), and differences between the baseline and H_2 internal combustion engine (H_2-ICE) scenarios (right: **c** and **f**). Data are averaged over the lowest model level (∼ 100 m). Note that the scales are different among panels.

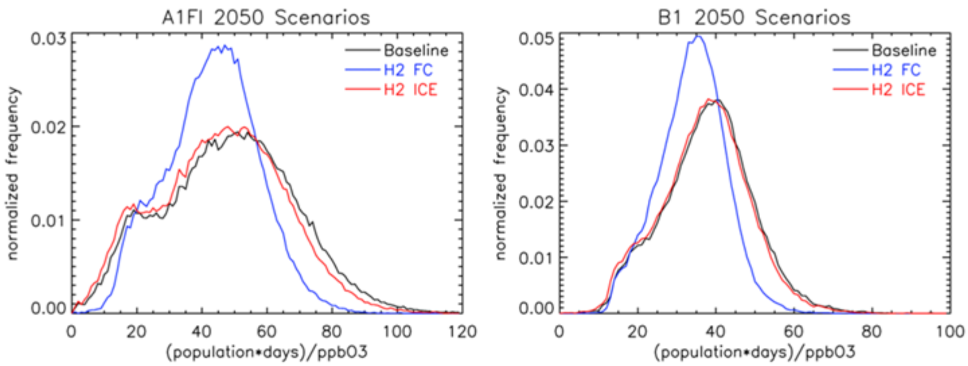

Fig. 6. Normalized probability distribution [population·days/ppb] of CMAQ simulated surface daily maximum 8 h-average O_3 concentrations throughout one year for the A1FI (left) and B1 (right) baseline, H_2-ICE, and H_2-FC scenarios across the United States. Distributions are based on the US population distribution for 2000 and the bin interval is 1 ppbv.

reductions are much less significant than in the H_2-FC scenario.

In the A1FI H_2-FC scenario, the population of the United States would experience considerably fewer days above the 75 ppb limit than in the baseline scenario (Fig. 6). Here, we perform an analysis of time cumulated population exposure to levels of ambient ozone using population data from the 2000 US census (http://www.esri.com/data/download/census2000-tigerline/index.html) and assuming the population distribution does not change significantly by 2050. There is a large shift towards lower O_3 concentrations for the H_2-FC scenarios for both the A1FI and B1 scenarios (Fig. 6). In the A1FI scenario much of the large tail area above 75 ppbv is reduced and compliance with the ozone air quality standard is much more frequent (Fig. 6). While the improvements for the H_2-FC scenarios are quite impressive, the H_2-ICE scenario provides almost no noticeable improvement. The distributions are extremely similar except for a small reduction in the > 75 ppbv tail. In the B1 scenarios (Fig. 6) the standard is rarely exceeded in any scenario, but still there are substantial improvements with the adoption of a fuel cell powered road sector.

The scenarios examined in this study suggest that summertime O_3 overb the contiguous United States is predominantly NO_x controlled. This highlights the importance of the utilization of non-combustion technologies in which NO_x emissions are avoided, e.g., fuel cells, towards improving O_3 air quality in a H_2-based road transportation sector.

4.3 The tropospheric oxidizing capacity (OH) and climate implication

As discussed in Sect. 1, utilization of H_2 raises concern over its potential impact on the oxidizing capacity of the troposphere. Our model simulations show that adoption of a H_2-based road transportation sector can either decrease or increase the tropospheric OH abundance (e.g., see Spivakovsky et al., 2000 for discussion of the climatology of tropospheric OH), depending on the technology option selected.

The tropospheric mean OH abundance changes from the 2000 modeled value of 9.7×10^5 molecules cm^{-3} to 9.1×10^5 molecules cm^{-3} in the 2050 A1FI baseline scenario (Table 1), mainly a result of the projected increase in CO emissions and CH_4 concentration in this scenario despite that the modeled tropospheric O_3 concentration increases. In contrast, the tropospheric mean OH abundance increases to 10.1×10^5 molecules cm^{-3} in the B1 baseline scenario (Table 2) due to the projected decreased CO emissions in this scenario.

The sensitivity study of the BL + H_2 scenarios suggests that H_2 leakage emission itself from a H_2-based road transportation sector can have some impact on tropospheric OH abundance, assuming a leakage rate of 2.5 %. The mean tropospheric OH abundance decreases by 2 % and 1 % in the A1FI and B1 scenarios, respectively, from the baseline scenarios (Tables 1 and 2). The reductions in OH abundance mainly occur in the tropical troposphere (Fig. 7a and d).

The combined effect of H_2 leakage emission and reductions in ozone precursor emissions in the A1FI and B1 H_2-FC scenarios is a 4 % decrease in the mean tropospheric OH abundance (Tables 1 and 2). The largest OH abundance reduction is in the tropical boundary layer and extends to the middle troposphere (Fig. 7b and e). However, the OH abundance increases in the remote troposphere at high latitudes in the NH as a result of its decreased sink against CO, as CO concentrations decrease there.

In the H_2-ICE scenarios the tropospheric OH abundance would actually increase by 7 % for the A1FI scenario and by 3 % for the B1 scenario (Tables 1 and 2) despite the increased atmospheric H_2 concentrations, which would reduce OH abundance by 2 %. This is likely because O_3 initiated OH production is not severely affected in these scenarios, while the OH sink through reactions with CO and other fossil fuel combustion byproducts is significantly reduced. The

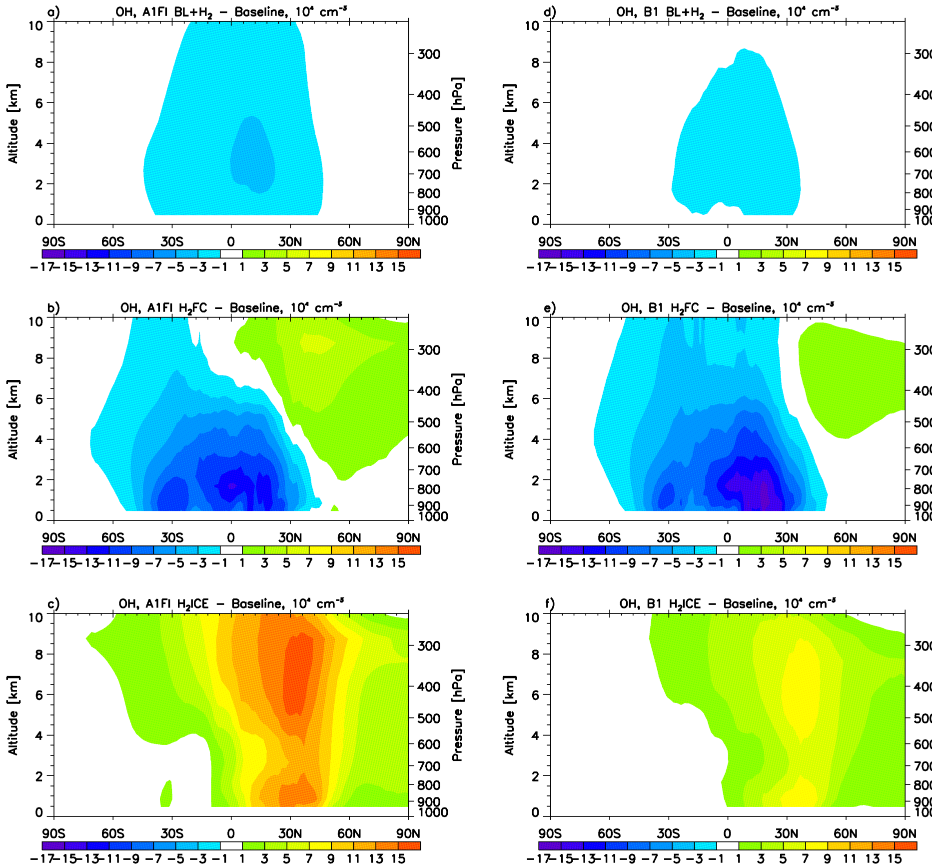

Fig. 7. CAM-Chem simulated 2050 annual averaged zonal-mean OH abundance differences in the H_2 BL + H_2, H_2-FC and the H_2-ICE scenarios from the corresponding BL scenarios (10^{-4} cm^{-3}). Note the different scales.

tropospheric OH abundance increases by 10 % and by 3 % in the NH and in the SH, respectively, in the A1FI H_2-ICE scenario (Fig. 7c), whereas it increases by 5 % and by 1 % in the NH and in the SH, respectively, in the B1 H_2-ICE scenario (Fig. 7f). Evidently the effect of the H_2 economy on global OH is relatively small for the scenarios examined here and can be positive or negative with relatively minor contributions to atmospheric chemistry and climate forcing, as discussed next.

Impact on CH_4 lifetime and climate

Since the reaction with OH is the primary sink of CH_4, changes in the OH abundance have direct impact on the atmospheric CH_4 lifetime. Here, the CH_4 lifetime was calculated by dividing the CH_4 tropospheric burden by its sink against OH. A companion run of the current atmosphere estimates CH_4 lifetime to be 8.7 yr, well within the 8∼ 10 yr range summarized by IPCC (2007). The baseline CH_4 lifetime is 9.1 yr for the A1FI scenario and 8.3 yr for the B1 scenario. In the 2050 H_2-FC scenarios, the CH_4 lifetimes increased by 7 % to 9.7 yr for the A1FI scenario and by 6 % to 8.8 yr in the B1 scenario. However, in the H_2-ICE scenarios, the CH_4 lifetime decreased by 4 % to 8.7 yr in the A1FI scenario and by 2 % to 8.1 yr in the B1 scenario. These changes imply that transitioning to a H_2 fuel cell type road transportation sector may exacerbate climate warming due to CH_4 through its increased lifetime. However, the amount of warming due to CH_4 will depend on its actual atmospheric concentrations, which will depend on many factors, including how any transition to a H_2 economy occurs, and also any changes in other, e.g., biogenic, CH_4 emissions that might occur (not evaluated here).

It is interesting to investigate the combined climate effects of a H_2-based road transportation sector in terms of both changes in CH_4 lifetime and changes in O_3 concentration. In the H_2-FC scenarios, the decrease in tropospheric ozone concentrations, which implies a cooling effect, is accompanied by an increase in CH_4 lifetime, which implies a warming effect. The two effects tend to offset each other, but the effect is inhomogeneous because tropospheric ozone is short-lived and is thus not uniform, whereas CH_4 is long-lived and uniform. The changes in aerosol loadings, especially for soot

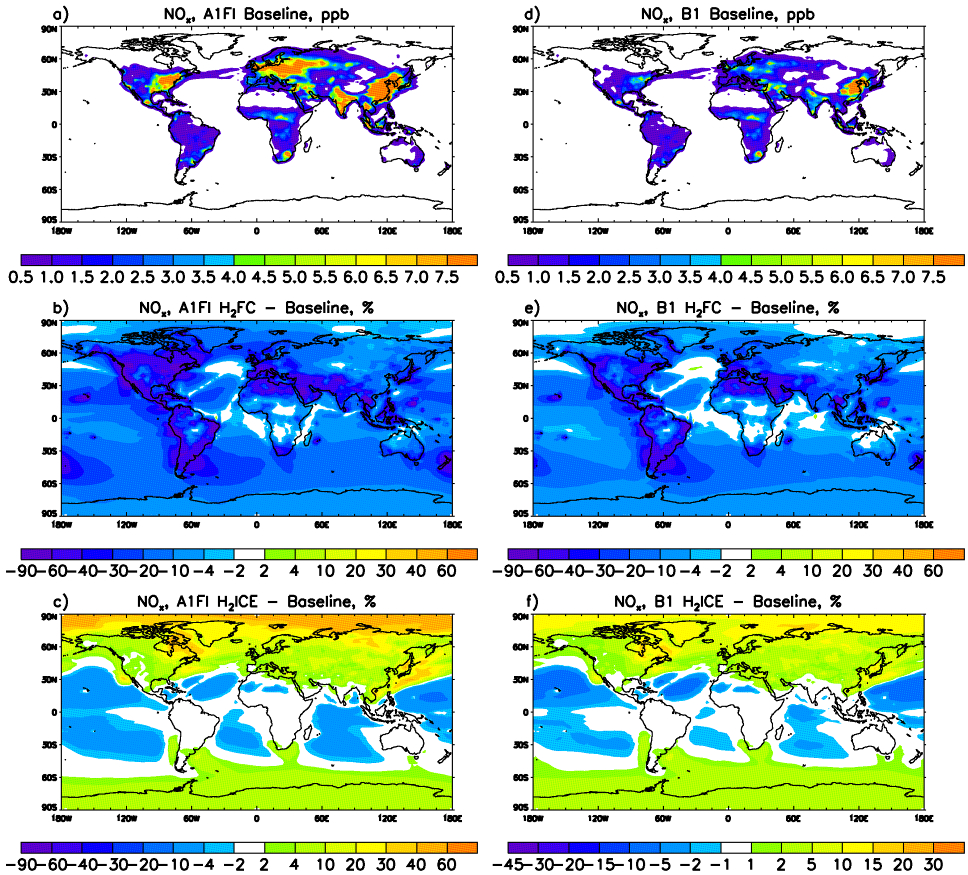

Fig. 8. CAM-Chem simulated 2050 annual mean surface NO_x mixing ratios in the A1FI **(a)** and B1 **(d)** baseline scenarios and percent differences for the H_2 fuel cell (H_2-FC) and H_2 internal combustion engine (H_2-ICE) scenarios **(b, c, e, f)**. Note the different scales.

and sulfate, would further complicate the combined climate effect problem of the H_2-FC scenarios.

Whereas in the H_2-ICE scenarios, both tropospheric ozone concentration and CH_4 lifetime are decreased, implicating a negative radiative forcing. Taking soot reductions enhances this cooling effect while reductions of sulfate aerosols would counteract it. Again, it is interesting to investigate the climate effect of the H_2-ICE scenarios because of its inhomogeneity.

4.4 NO_x

The tropospheric NO_x burden depends on the type of H_2 technology option selected. In the H_2-FC scenarios tropospheric NO_x concentrations are reduced significantly, by 16 % in the A1FI scenario and by 11 % in the B1 scenario (Tables 1 and 2). In the H_2-ICE scenarios; however, tropospheric NO_x concentrations increase by 10 % in the A1FI scenario and by 3 % in the B1 scenario.

Regions with intense human activities, such as eastern China, India, northeastern United States, and Western Europe, have high NO_x concentrations in the baseline scenarios (Fig. 8a and d). These regions would benefit substantially from NO_x reductions in the A1FI H_2-FC scenario. Annual mean ground-level NO_x concentrations decrease considerably along the coasts of North and South America, Western Europe, North Africa, the Middle East, New Zealand, and Japan (Fig. 8b), with percentage reductions as high as 80 %. Although some remote areas have large relative changes, for example much of the remote Southern Hemisphere, the absolute changes are quite small there as the baseline NO_x mixing ratio is rather low. The relative reductions are most pronounced in wintertime, when the boundary layer height is lower and ventilation is inhibited. In the B1 H_2-FC scenario, the reduction in NO_x concentrations occurs in the same regions, but the percentages are about half of those in the A1FI scenario (Fig. 8e).

In the A1FI and B1 H_2-ICE scenarios the simulated surface NO_x concentration change is not apparent in the NO_x pollution areas (Fig. 8c and f), showing that the internal combustion engine type of H_2-based road transportation sector would not be as effective in ground-level NO_x mitigation.

As in the global CAM-Chem simulations, the CMAQ model results show that higher NO_x concentrations tend to appear in wintertime, so here we focus on the wintertime

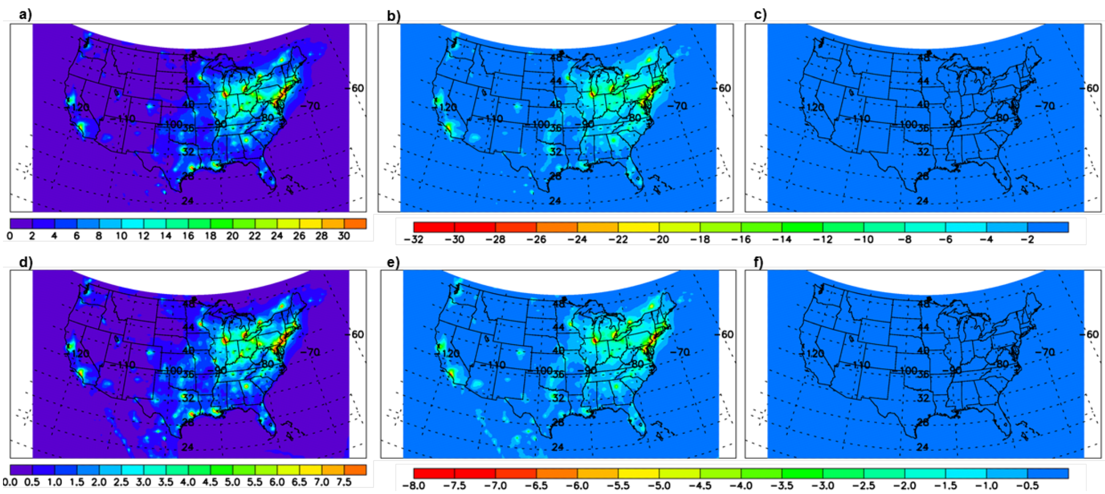

Fig. 9. February 2050 average NO_x concentrations (ppbv) simulated by CMAQ for the A1FI (top) and B1 scenarios (bottom). Each row contains the BL scenarios (left: **a** and **d**), differences (ppbv) between the BL and H_2-FC scenarios (center: **b** and **e**), and differences (ppbv) between the BL and H_2-ICE scenarios (right: **c** and **f**). Data are from the lowest model level (∼ 100 m). Note that the scales are different among panels.

(February) changes. NO_x peaks are concentrated in the northeastern United States and in locations in the west, e.g., Los Angeles and the San Francisco Bay Area of California (Fig. 9a and d). Wintertime concentrations are higher than summertime concentrations and concentrations are higher in the A1FI than B1 scenarios. There are large decreases in NO_x concentrations with the adoption of a H_2 fuel cell transportation sector (Fig. 9b and e), up to ∼ 13 ppbv (∼ 50 %) in winter over the northeast United States for the A1FI scenario. However, for the H_2-ICE scenario there is almost no change in wintertime NO_x concentrations evident (Fig. 9c and f).

4.5 CO

The tropospheric CO burdens decrease by 14 % and 18 % for the A1FI H_2-FC and H_2-ICE scenarios, respectively, and by 4 % and 7 % for the B1 H_2-FC and H_2-ICE scenarios, respectively (Tables 1 and 2).

In the A1FI baseline scenario, annual mean surface CO concentrations over North America and Eurasia exceed 200 ppbv (Fig. 10a). Higher values are present in the northeastern US, Central Europe and eastern China. There are also higher than background concentrations in the tropics due to biomass burning. In the B1 baseline scenario, annual mean surface CO concentrations over the NH continents are over 100 ppbv (Fig. 10b). Higher concentrations are seen in eastern China, northeastern US, and tropical regions.

In the A1FI H_2-FC scenario, surface CO concentrations in remote areas of the NH decrease by at least 20 % (Fig. 10b). Relative CO concentration reductions in the H_2-FC scenario are largest in hotspots of human activities, such as northeastern US, California, central and western Europe, eastern China, South Korea and Japan. Concentrations in New York City decrease by as much as 80 %. The CO mitigation is perennial but is most pronounced in winter. In the H_2-ICE scenario the ground-level CO concentration reduction pattern is similar to that in the A1FI H_2-FC scenario, but the magnitude of reduction is even larger (Fig. 10c) due to ∼ 11 % higher OH concentrations in the A1FI H_2-ICE scenario than the A1FI H_2-FC scenario. This is a result of the increase in atmospheric oxidizing capacity in the H_2 internal combustion engine scenarios, which would lead to decreases in species that react with OH, e.g., CO and other VOCs.

In the B1 H_2-FC and H_2-ICE scenarios, the background CO concentrations in the NH decrease by 10–20 % relative to the baseline scenario (Fig. 10d–f). The largest relative reduction (up to 50 %) appears over northeastern United States. There is also a 30 % decrease in Western Europe. The relative and absolute CO decreases in B1 H_2 scenarios are smaller than those in the corresponding A1FI scenarios.

The regional US CMAQ simulations are consistent with the CAM-Chem global simulations for 2050. Baseline CO concentrations are generally highest over the US east coast in wintertime, with monthly average wintertime concentrations of greater than 400 ppbv and 150 ppbv over much of the eastern part of the United States in the A1FI and B1 scenarios, respectively (Fig. 11a and d). However, analysis shows that there is no violation of CO NAAQS, that is, 8 h average not to exceed 9 ppmv and 1 h average not to exceed 35 ppmv more than once per year, in any of the scenarios examined. In the H_2-FC and H_2-ICE scenarios there are large decreases in CO concentrations due to the decrease in CO emissions. The largest decreases occur over areas with the highest emissions in the baseline scenario and, in contrast

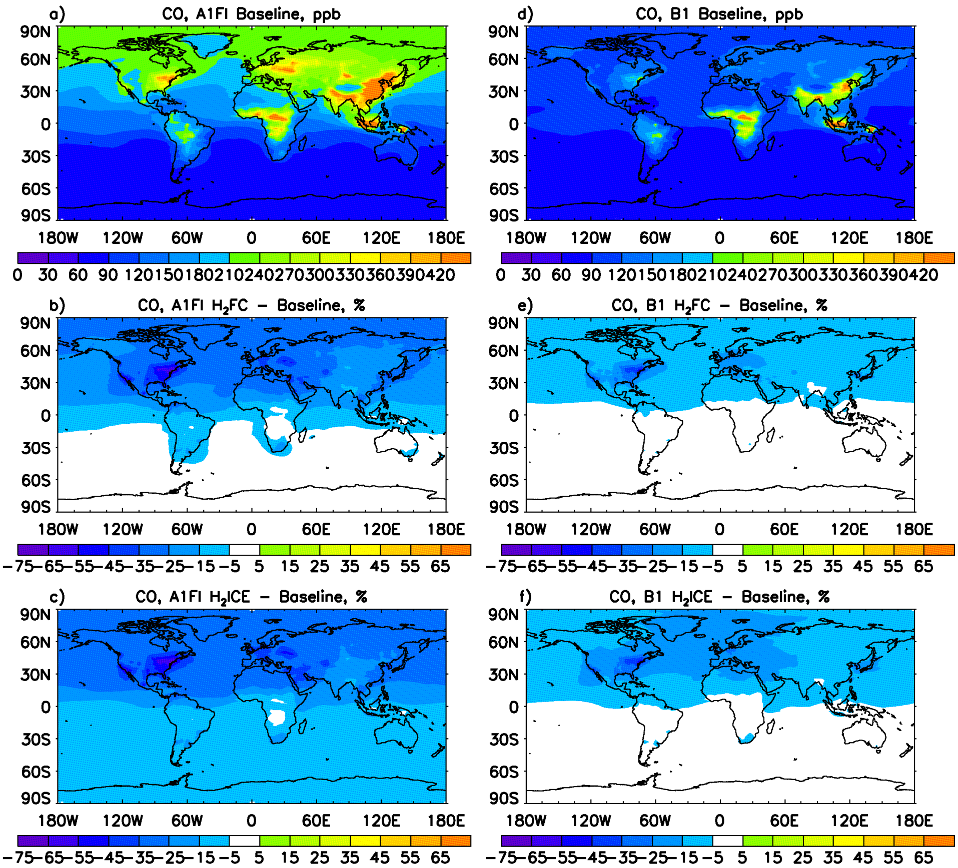

Fig. 10. CAM-Chem simulated 2050 annual mean surface CO mixing ratios in the A1FI **(a)** and B1 **(d)** baseline scenarios and percent differences for the H_2 fuel cell (H_2-FC) and H_2 internal combustion engine (H_2-ICE) scenarios **(b, c, e, f)**. Note the different scales.

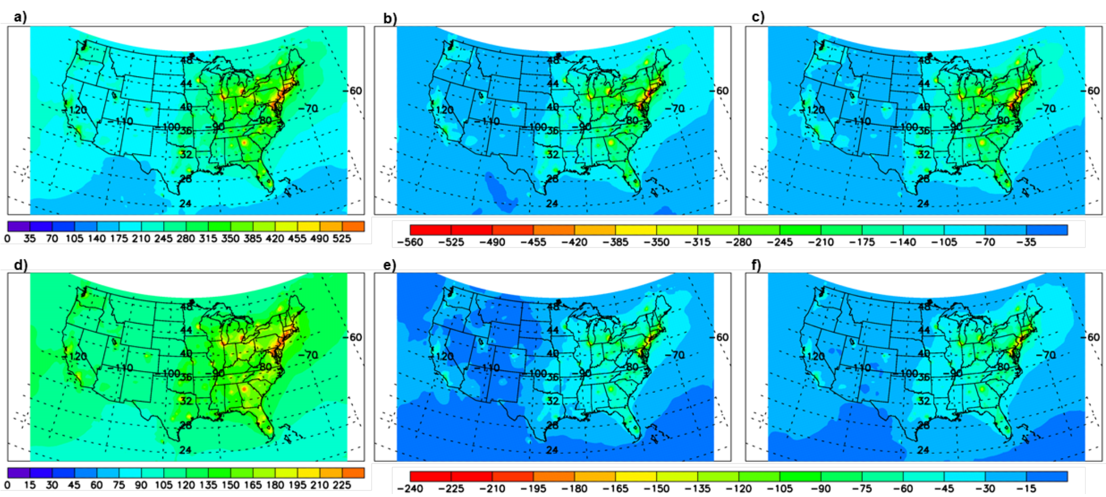

Fig. 11. February 2050 averages CO concentrations (ppbv) simulated by CMAQ for the A1FI (top) and B1 scenarios (bottom). Each row contains the BL scenarios (left: **a** and **d**), differences (ppbv) between the BL and H_2-FC scenarios (center: **b** and **e**), and differences (ppbv) between the BL and H_2-ICE scenarios (right: **c** and **f**). Data are from the lowest model level (∼ 100 m). Note that the scales are different among panels.

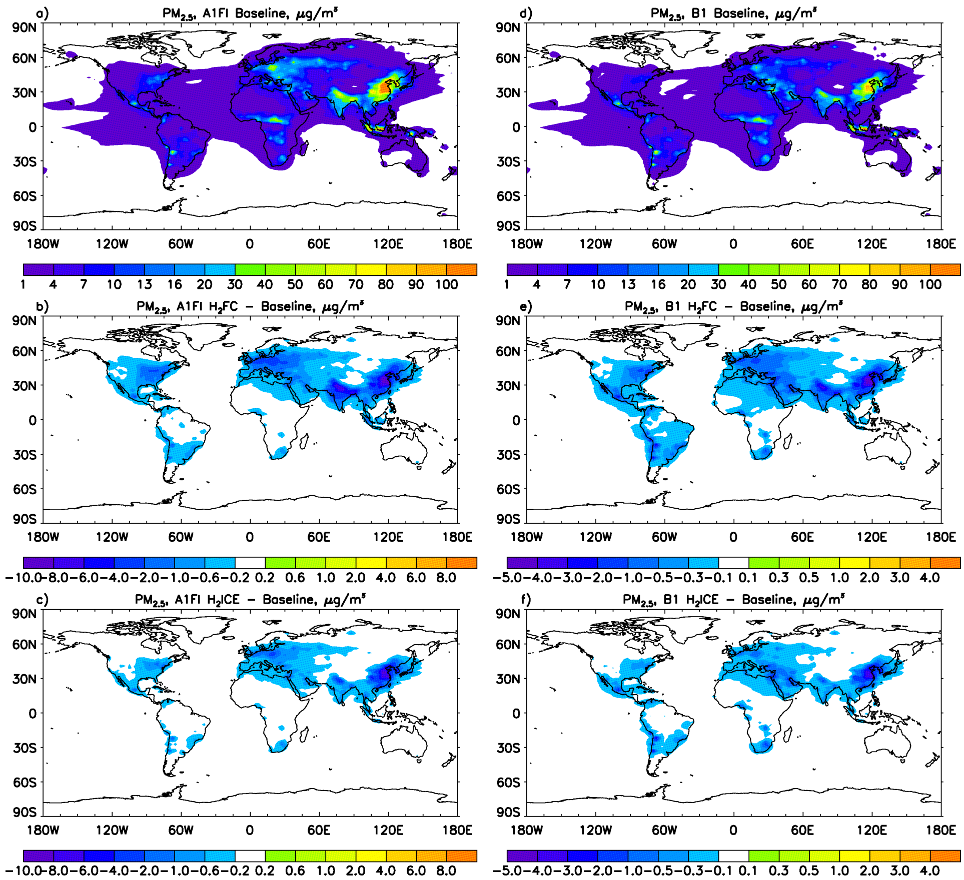

Fig. 12. CAM-Chem simulated 2050 annual mean surface $PM_{2.5}$ concentrations in the A1FI **(a)** and B1 **(d)** baseline scenarios and differences for the H_2 fuel cell (H_2-FC) and H_2 internal combustion engine (H_2-ICE) scenarios **(b, c, e, f)**. Note the different scales.

to some other pollutants, there are only slight differences between the H_2-FC and H_2-ICE scenarios. Wintertime CO decreases are nearly 280 ppbv and 100 ppbv for the A1FI and B1 scenarios over polluted regions, corresponding to decreases over much of the US east coast of greater than 60 % (Fig. 11b, c, e and f). Summertime decreases are nearly half as large as wintertime decreases (not shown) because the wintertime planetary boundary layer is shallower, there is less vigorous vertical mixing, and chemical loss is lower.

4.6 Aerosols

In the H_2-FC scenarios, tropospheric aerosols, especially soot, sulfate aerosols and ammonium nitrate concentrations are significantly reduced as a result of emissions decreases. In the H_2-ICE scenarios, tropospheric soot and sulfate aerosol concentrations decrease while ammonium nitrate aerosol concentrations increase due to the NO_x concentration increase.

In CAM-Chem, $PM_{2.5}$ includes sulfate aerosol, nitrate aerosol, black carbon, organic carbon, secondary organic aerosol, and dust and sea salt aerosols with diameters no larger than 2.5 µm. Since emission changes have little impact on dust and sea salt aerosols, we exclude these types of aerosols in the following discussion of $PM_{2.5}$.

Figure 12a and d show the CAM-Chem simulated annual mean surface $PM_{2.5}$ concentrations in the A1FI and B1 BL scenarios. In the A1FI BL scenario, eastern China is subject to high $PM_{2.5}$ concentrations of more than 100 µg m^{-3}. Surface $PM_{2.5}$ concentrations can be as high as 50 µg m^{-3} in northern India and parts of Indonesia. In central Europe, near ground $PM_{2.5}$ concentrations reach 30 µg m^{-3}. In the eastern United States, surface $PM_{2.5}$ concentrations are 10–20 µg m^{-3}. Annual mean surface $PM_{2.5}$ concentrations in the B1 BL scenario (Fig. 12d) are generally lower than those in the A1FI BL scenario. In central Europe and eastern United States it is ∼ 10 µg m^{-3} lower, whereas in eastern China it can be ∼ 50 µg m^{-3} lower than in the A1FI BL scenario.

In the A1FI H_2-FC scenario, annual mean surface $PM_{2.5}$ concentrations are significantly reduced in eastern China and northern India, by up to 10 µg m^{-3} (Fig. 12b). In northeastern United States and Europe, $PM_{2.5}$ concentrations are reduced by 1–3 µg m^{-3}. In the A1FI H_2-ICE scenario, surface $PM_{2.5}$

concentrations reductions in the northeastern United States, India and Europe are not as significant as in the A1FI H_2-FC scenario, whereas the reductions in eastern China is comparable to the A1FI H_2-FC scenario (Fig. 12c).

In the B1 H_2-FC scenario, there are only a few locations with annual mean surface $PM_{2.5}$ concentrations reductions of more than 1 $\mu g\,m^{-3}$ (Fig. 12e). The maximum reduction of $\sim 5\,\mu g\,m^{-3}$ appears in eastern China. In the B1 H_2-ICE scenario, surface $PM_{2.5}$ concentrations reductions are even less significant than in the B1 H_2-FC scenario. Higher reductions are only seen in eastern China (Fig. 12f).

Again, the regional US CMAQ simulations are consistent with the global CAM-Chem simulations but with more localized peaks due to their higher resolution. In the A1FI and B1 baseline scenarios, the only location in the contiguous US exceeding the annual mean $PM_{2.5}$ NAAQS (15 $\mu g\,m^{-3}$) is around Buffalo, NY. In the H_2-FC and H_2-ICE scenarios in both the A1FI and B1 scenarios, annual mean $PM_{2.5}$ concentration in Buffalo, NY, decreases but it is still above the NAAQS.

$PM_{2.5}$ concentrations are typically higher in winter than in summer. For the baseline A1FI and B1 scenarios, highest $PM_{2.5}$ concentrations over the contiguous United States appear generally along the Ohio River Valley and the East Coast (Fig. 13a and d). February average surface concentrations peak at roughly 9 $\mu g\,m^{-3}$ for the A1FI scenario and around 8 $\mu g\,m^{-3}$ for the B1 scenario. As with O_3, improvements in $PM_{2.5}$ air quality depend on the technology adoption scenario. $PM_{2.5}$ reductions are greatest with the H_2-FC scenarios' NO_x and VOC emissions reductions, while the reductions are much more modest with the VOC only emissions reductions of the H_2-ICE scenario. While the areas of largest absolute decrease correspond to the areas of highest initial concentrations, the areas of largest relative decrease are typically over areas with lower initial concentrations in the Midwest and west coast. For the H_2-FC scenario there are reductions of $\sim 1.5\,\mu g\,m^{-3}$ and $\sim 1\,\mu g\,m^{-3}$ for the A1FI and B1 scenarios in February over the regions of high concentration in the Midwest (Fig. 13b and e). For the H_2-ICE scenario, reductions are much more modest at around 1 and 0.5 $\mu g\,m^{-3}$ for the A1FI and B1 scenarios, respectively, and more concentrated on the eastern seaboard (Fig. 13c and f). The smaller $PM_{2.5}$ reduction in the H_2-ICE scenarios is primarily due to the impact of nitrate aerosol $PM_{2.5}$ production from the NO_x emissions, whereas in the H_2-FC scenario there are reductions in soot, sulfate, and nitrate aerosols as well as secondary organic aerosol formation from decreases in VOC emissions.

The changes in annual mean surface PM_{10} concentrations (not shown) are the same as those for $PM_{2.5}$, because the diameters of the aerosols reduced are less than 2.5 µm in the CAM-Chem simulation. The following sections discuss the aerosol components that are significantly reduced.

4.6.1 Soot

In the baseline scenarios, soot (black carbon) concentrations at the surface are rather low in remote regions (less than 1 $\mu gC\,m^{-3}$) (Fig. 14a and d). It is nearly absent in the air of pristine regions (concentrations less than 0.1 $\mu gC\,m^{-3}$). In the tropics, soot concentrations are higher due to biomass burning. Densely populated regions are plagued with soot pollution from intense fossil fuel combustion activities. These regions include eastern China, Europe, North America, Korea, Japan, and India. The worst pollution occurs in eastern China, where annual mean soot concentration can be up to more than 10 $\mu gC\,m^{-3}$ in the A1FI BL scenario.

The tropospheric soot burden would decrease by 17 % and 7 % in the A1FI and B1 scenarios, respectively (Tables 1 and 2), both in the H_2-FC and the H_2-ICE scenarios. Ground-level soot would be significantly reduced in most of the United States, Europe, and Japan (Fig. 14b, c, e and f). In the A1FI scenario a H_2-based road transportation sector reduces surface soot concentrations by as much as 50 % in the United States and Western Europe (Fig. 14b). Soot concentrations are also reduced by 30–40 % in the North Atlantic Ocean region and other regions downwind of key polluted areas. There is also significant relative reduction (~ 20 %) of soot in eastern China. The pattern of surface soot concentration reduction is almost identical in the A1FI H_2-ICE scenario to that in the A1FI H_2-FC scenario (Fig. 14c). In the B1 scenarios, soot reductions in the H_2-FC and H_2-ICE scenarios are 10–20 % less than in the corresponding A1FI scenarios, but they are still significant reductions and bear a similar pattern (Fig. 14e and f).

Soot is a warming climate agent (IPCC, 2001), though there remain uncertainties in quantitative understandings. Reductions of tropospheric soot, as in with a H_2-based road transportation sector, would have a cooling effect on climate. This effect would be inhomogeneous since the reduction is not uniform.

4.6.2 Sulfate aerosols

Sulfate aerosols (SO_4) are associated with human activities (Fig. 15a and d). The highest annual mean surface concentrations ($\sim 10\,\mu gSO_4\,m^{-3}$) are seen in eastern China, India, and Mexico in the A1FI BL scenario. In the B1 BL scenario, sulfate aerosol pollution in these densely populated areas is slightly less severe than in the A1FI BL scenario.

The tropospheric sulfate aerosol burdens decrease by 4 % for both the A1FI and B1 H_2-FC scenarios (Tables 1 and 2). In the A1FI H_2-FC scenario, surface SO_4 mass concentrations decrease by approximately 5 % around the world. Higher reductions of ~ 10 % occur in southern California, Southeast Asia and New Zealand (Fig. 15b). The increase in Antarctica is not significant as the background sulfate aerosol concentration is extremely small there (less than 0.1 $\mu g\,SO_4\,m^{-3}$) (Fig. 15a and d).

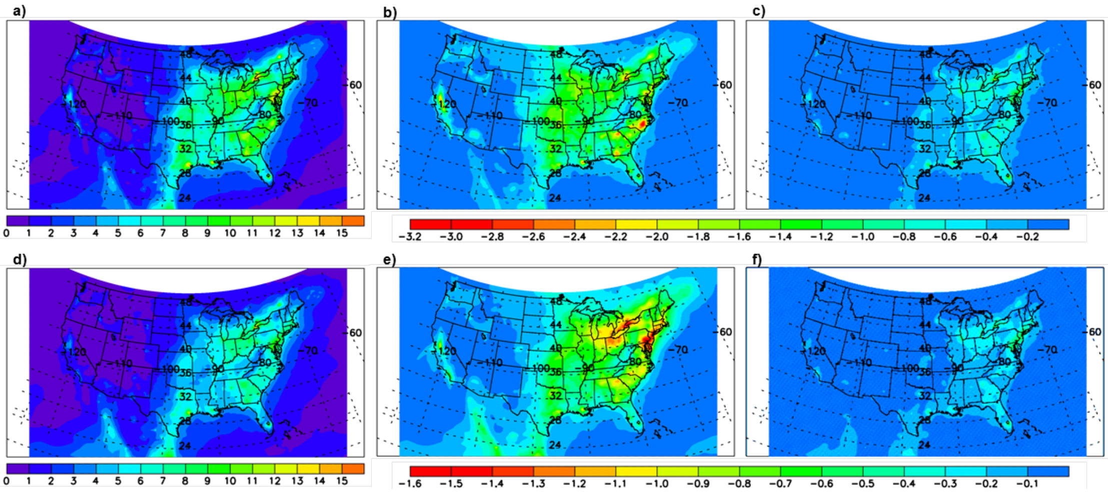

Fig. 13. February 2050 average $PM_{2.5}$ concentrations ($\mu g\,m^{-3}$) simulated by CMAQ for the A1FI (top) and B1 scenarios (bottom). Each row contains the BL scenarios (left: **a** and **d**), differences ($\mu g\,m^{-3}$) between the BL and H_2-FC scenarios (center: **b** and **e**), and differences ($\mu g\,m^{-3}$) between the BL and H_2-ICE scenarios (right: **c** and **f**). Data are from the lowest model level ($\sim$ 100 m). Note that the scales are different among panels.

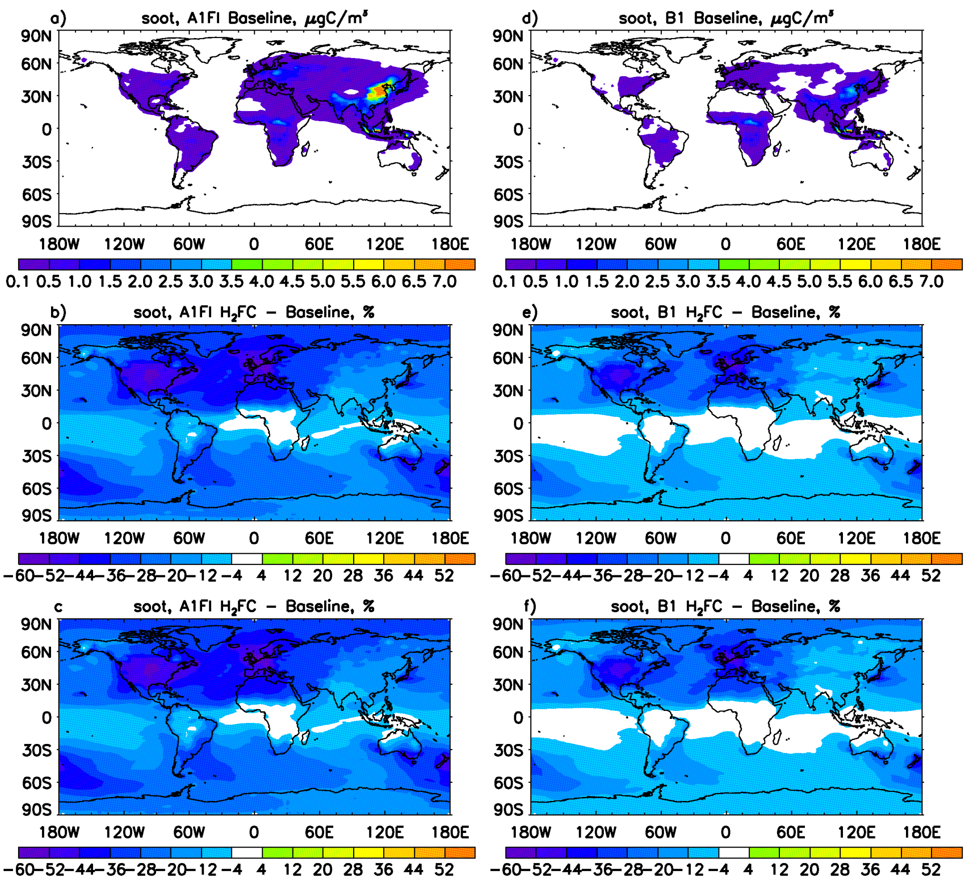

Fig. 14. CAM-Chem simulated 2050 annual mean surface soot concentrations in the A1FI **(a)** and B1 **(d)** baseline scenarios and percent differences for the H_2 fuel cell (H_2-FC) and H_2 internal combustion engine (H_2-ICE) scenarios **(b, c, e, f)**. Note the different scales.

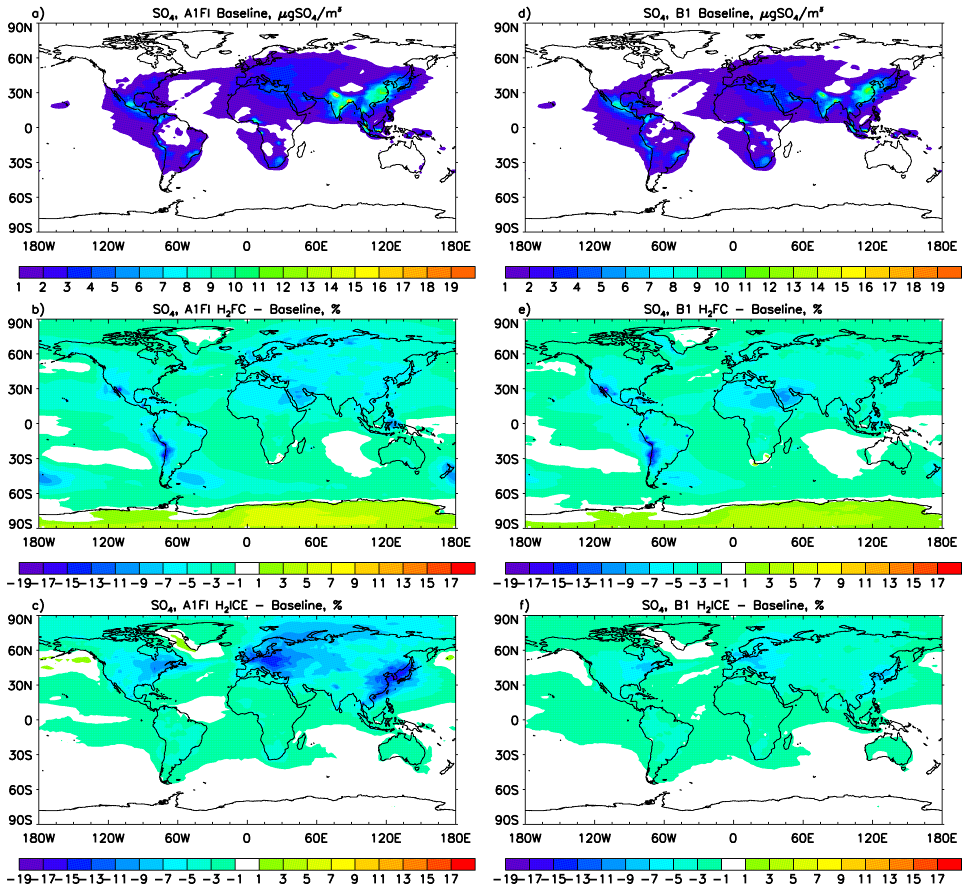

Fig. 15. CAM-Chem simulated 2050 annual mean surface SO_4 concentrations in the A1FI **(a)** and B1 **(d)** baseline scenarios and percent differences for the H_2 fuel cell (H_2-FC) and H_2 internal combustion engine (H_2-ICE) scenarios **(b, c, e, f)**. Note the different scales.

The tropospheric sulfate aerosol burdens decrease by 3 % for the two H_2-ICE scenarios. In the A1FI H_2-ICE scenario, there is around 10–15 % decrease in SO_4 mass concentration over most Eurasia, North Africa, western United States, Mexico, and South America (Fig. 15c). The H_2-ICE scenario is slightly less powerful than the H_2-FC scenario in SO_4 mitigation (Fig. 15f) because the former has greater oxidizing power, which makes the oxidation of SO_2 to sulfate aerosols faster than in the latter scenario.

4.6.3 Ammonium nitrate

In 2050, as today, annual mean surface ammonium nitrate aerosols (NH_4NO_3) concentrations are higher in regions with intense human activities, such as the northeastern United States, Europe and eastern China and India (Fig. 16a and d). The highest annual mean surface concentrations ($\sim 10\,\mu g\,m^{-3}$) are seen in eastern China and India in the A1FI BL scenarios. Surface ammonium nitrate aerosols concentrations are slightly lower in the B1 BL scenarios than in the A1FI.

The tropospheric ammonium nitrate aerosol burdens decrease by 12 % and by 9 % in the A1FI and B1 H_2-FC scenarios, respectively (Tables 1 and 2). In the A1FI H_2-FC scenario, surface concentrations decrease significantly around the world. Concentrations decrease by as much as 80 %, for example, in California (Fig. 16b). Reductions are nearly as significant in the B1 H_2-FC scenario as in the A1FI H_2-FC scenario in terms of percent change (Fig. 16e).

The tropospheric ammonium nitrate aerosol burdens increase by 3 % and by 2 % in the A1FI and B1 H_2-ICE scenarios, respectively (Tables 1 and 2). Surface concentrations increase in remote regions (Fig. 16a and d) as a result of the increased NO_x concentrations there (see Sect. 4.4). In the A1FI H_2-FC scenario, there are slight concentration reductions (~ 10 %) in the Ohio River Valley and in eastern China (Fig. 16b). The relative increase in remote regions is not significant because the background concentration is extremely small there (less than $0.1\,\mu g\,m^{-3}$) (Fig. 16a and d).

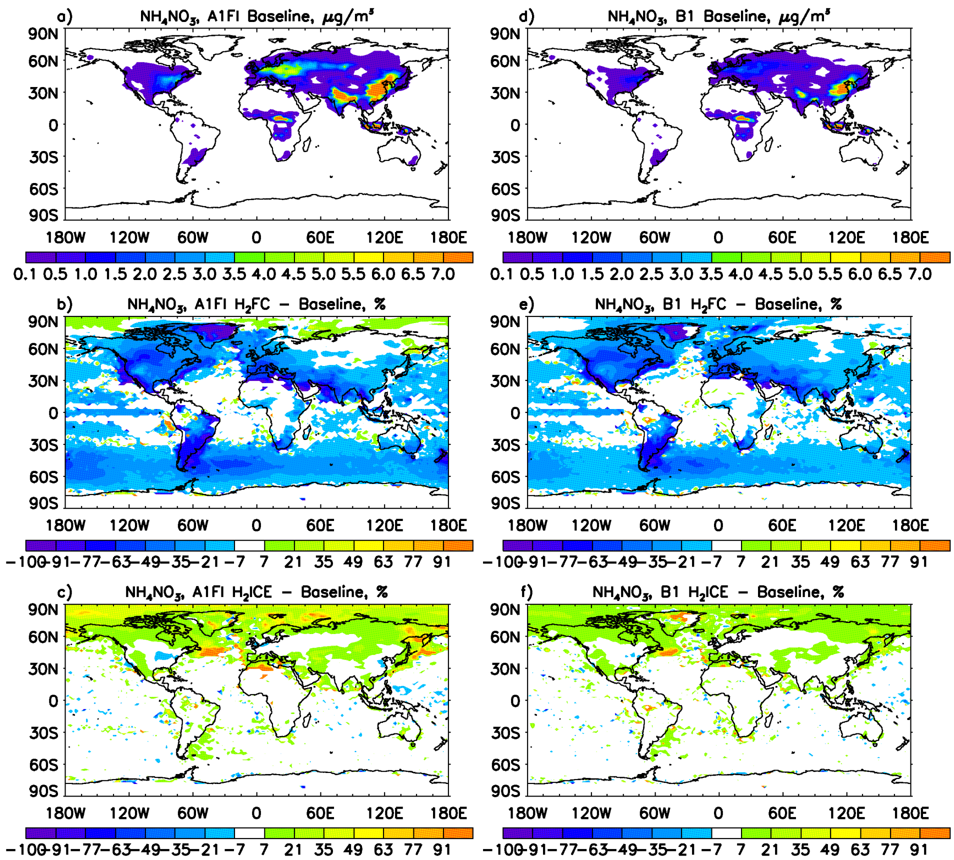

Fig. 16. CAM-Chem simulated 2050 annual mean surface NH_4NO_3 concentrations in the A1FI **(a)** and B1 **(d)** baseline scenarios and percent differences for the H_2 fuel cell (H_2-FC) and H_2 internal combustion engine (H_2-ICE) scenarios **(b, c, e, f)**. Note the different scales.

5 Conclusions

We have evaluated the possible impacts of transitioning to a H_2 powered road transportation sector in 2050 using atmospheric chemistry-climate models and emissions scenarios based on the IPCC A1FI and B1 SRES growth scenarios and fuel cell and internal combustion engine technology options. Our results show that air quality would improve significantly with adoption of a H_2 fuel cell type road transportation sector (H_2-FC scenarios). Primary gaseous (CO, NO_x) and particulate (soot) pollutants are reduced substantially once the fossil fuel-based road transportation sector transitions to H_2 fuel cells. Ozone, a major secondary pollutant that often exceeds air quality standards in some regions of the United States (and is a severe problem in developing countries), would be reduced to a significant extent as its precursors, CO, NO_x and NMVOCs emissions, are reduced. Additionally, concentrations of particulate matter, especially those with diameters less than 2.5 µm ($PM_{2.5}$), would be significantly reduced in densely populated regions.

Some aspects of air quality would also improve with application of a H_2 internal combustion engine type road transportation sector (H_2-ICE scenarios). Ambient ozone concentrations would decrease slightly as its precursor emissions by fossil fuel combustion from the road transportation sector are eliminated. Ozone mitigation with the H_2-ICE option is not nearly as effective as in the H_2-FC scenarios but is somewhat more effective in the relatively few VOC-limited regions. Urban $PM_{2.5}$ concentrations would not be significantly reduced except in eastern China.

For each specific type of H_2 technology applied in the road transportation sector, the reductions of key air pollution species are not as significant in the B1 scenario as in the A1FI scenario. However, since the emissions of key ozone and aerosol precursors are lower in the B1 scenarios, air quality in the B1 scenarios is generally better than that in the A1FI scenarios. For example, tropospheric ozone concentrations are substantially lower in all of the B1 scenarios than in all of the A1FI scenarios regardless of the H_2 technology adopted.

With a leakage rate of 2.5 %, H_2 emissions in a H_2-based road transportation sector are larger than the replaced H_2 emissions from fossil fuel burning, leading to increased H_2 concentrations in the atmosphere. The added H_2 would decrease tropospheric OH abundance, resulting in elongated

CH_4 lifetime and thus warming. However, when taking changes in emissions of CO, NO_x and NMVOCs into account, the picture of the climate impact is more complicated. In the H_2-FC scenarios, the combined effect of emission changes is a 4 % decrease in OH abundance, which contributes to warming by increasing CH_4 lifetime. On the other hand, concurrent decrease in tropospheric O_3 concentrations would provide a cooling mechanism. The overall effect is further complicated by the temporal and spatial inhomogeneity of the two offsetting mechanisms. In the H_2-ICE scenarios, both decrease in CH_4 lifetime due to OH increase and the decrease in tropospheric O_3 tend to cool the climate, while, again, inhomogeneities in space and time would complicate the problem.

It is worth noting that our emission scenarios assumed 100 % market penetration of H_2 technologies in 2050. That is, all vehicles operating on the road are replaced with H_2 powered ones. We also assumed that the H_2 for road transportation was produced by renewable, nuclear, or fossil fuel facilities with advanced scrubbing technologies and with no emissions associated with its production. The positive and negative impacts presented here will decrease in magnitude to the extent that market penetration is not total and also whether there are emissions associated with H_2 production.

Acknowledgements. The authors thank Hugh Pitcher for providing projections of energy efficiency. Funding for this study was provided by the United States Department of Energy through award number DE-FC36-07GO17109 to the University of Illinois project "Evaluation of the Potential Environmental Impacts from Large-Scale Use and Production of Hydrogen in Energy and Transportation Applications". MKD thanks Los Alamos National Laboratory's LDRD and IGPP for nurturing this research.

Edited by: D. Shindell

References

Abe, R.: Recent progress on photocatalytic and photoelectrochemical water splitting under visible light irradiation, J. Photoch. Photobio. C, 11, 179–209, 2010.

Appel, K. W., Gilliland, A. B., Sarwar, G., and Gilliam, R. C.: Evaluation of the Community Multiscale Air Quality (CMAQ) model version 4.5: Sensitivities impacting model performance Part I – Ozone, Atmos. Environ., 41, 9603–9615, 2007.

Appel, K. W., Bhave, P. V., Gilliland, A. B., Sarwar, G., and Roselle, S. J.: Evaluation of the community multiscale air quality (CMAQ) model version 4.5: Sensitivities impacting model performance; Part II – particulate matter, Atmos. Environ., 42, 6057–6066, 2008.

Barnes, D. H., Wofsy, S. C., Fehlau, B. P., Gottlieb, E. W., Elkins, J. W., Dutton, G. S., and Novelli, P. C.: Hydrogen in the atmosphere: Observations above a forest canopy in a polluted environment, J. Geophys. Res., 108, doi:10.1029/2001JD001199, 2003.

Bond, T. C., Streets, D. G., Yarber, K. F., Nelson, S. M., Woo, J. H., and Klimont, Z.: A technology-based global inventory of black and organic carbon emissions from combustion, J. Geophys. Res., 109, D14203, doi:10.1029/2003JD003697, 2004.

Byun, D. and Schere, K. L.: Review of the governing equations, computational algorithms, and other components of the models-3 Community Multiscale Air Quality (CMAQ) modeling system, Appl. Mech. Rev., 59, 51–77, 2006.

Colella, W. G., Jacobson, M. Z., and Golden, D. M.: Switching to a US hydrogen fuel cell vehicle fleet: The resultant change in emissions, energy use, and greenhouse gases, J. Power Sources, 150, 150–181, 2005.

Conrad, R. and Seiler, W.: Influence of Temperature, Moisture, and Organic-Carbon on the Flux of H_2 and CO between Soil and Atmosphere: Field Studies in Sub-Tropical Regions, J. Geophys. Res., 90, 5699–5709, 1985.

Constant, P., Poissant, L., and Villemur, R.: Annual hydrogen, carbon monoxide and carbon dioxide concentrations and surface to air exchanges in a rural area (Québec, Canada), Atmos. Environ., 42, 5090–5100, 2008.

Constant, P., Poissant, L., and Villemur, R.: Tropospheric H_2 budget and the response of its soil uptake under the changing environment, Sci. Total Environ., 407, 1809–1823, 2009.

Derwent, R., Simmonds, P., O'Doherty, S., Manning, A., Collins, W., and Stenvenson, D.: Global environmental impacts of the hydrogen economy, Int. J. Nucl. Hydrogen Prod. Appl., 1, 57–67, 2006.

Ehhalt, D. H. and Rohrer, F.: The tropospheric cycle of H_2: a critical review, Tellus B, 61, 500–535, 2009.

Granier, C., Lamarque, J. F., Mieville, A., Muller, J. F., Olivier, J., Orlando J., Peters, J., Petron, G., Tyndall, G., and Wallens, S.: POET, a database of surface emissions of ozone precursors, available at: http://www.aero.jussieu.fr/projet/ACCENT/POET.php, 2005.

Horowitz, L. W., Walters, S., Mauzerall, D. L., Emmons, L. K., Rasch, P. J., Granier, C., Tie, X. X., Lamarque, J. F., Schultz, M. G., Tyndall, G. S., Orlando, J. J., and Brasseur, G. P.: A global simulation of tropospheric ozone and related tracers: Description and evaluation of MOZART, version 2, J. Geophys. Res., 108, doi:10.1029/2002JD00285, 2003.

Huang, H. C., Lin, J. T., Tao, Z. N., Choi, H., Patten, K., Kunkel, K., Xu, M., Zhu, J. H., Liang, X. Z., Williams, A., Caughey, M., Wuebbles, D. J., and Wang, J. L.: Impacts of long-range transport of global pollutants and precursor gases on US air quality under future climatic conditions, J. Geophys. Res., 113, D19307, doi:10.1029/2007JD009469, 2008.

Intergovernmental Panel on Climate Change (IPCC): Special Report on Emissions Scenarios. Working Group III, IPCC, Cambridge University Press, Cambridge, 2000.

Intergovernmental Panel on Climate Change (IPCC): Climate Change 2001, the Scientific Basis. Contribution of Working Group 1 to the Third Assessment Report of the IPCC, Cambridge University Press, Cambridge, UK and New York, NY, USA, 881 pp., 2001.

Intergovernmental Panel on Climate Change (IPCC): Climate Change 2007, the Scientific Basis. Contribution of Working Group 1 to the Fourth Assessment Report of the IPCC, Cambridge University Press, Cambridge, UK and New York, NY, USA, 996 pp., 2007.

Jacob, D.: Introduction to Atmospheric Chemistry, Princeton University Press, Princeton, New Jersey, 1999.

Jacobson, M. Z.: Effects of wind-powered hydrogen fuel cell vehicles on stratospheric ozone and global climate, Geophys. Res. Lett., 35, L19803, doi:10.1029/2008GL035102, 2008.

Jacobson, M. Z., Colella, W. G., and Golden, D. M.: Cleaning the air and improving health with hydrogen fuel-cell vehicles, Science, 308, 1901–1905, 2005.

Kim, Y. and Logan, B. E.: Hydrogen production from inexhaustible supplies of fresh and salt water using microbial reverse-electrodialysis electrolysis cells, P. Natl. Acad. Sci. USA, 108, 16176–16181, 2011.

Lamarque, J. F., Kiehl, J. T., Hess, P. G., Collins, W. D., Emmons, L. K., Ginoux, P., Luo, C., and Tie, X. X.: Response of a coupled chemistry-climate model to changes in aerosol emissions: Global impact on the hydrological cycle and the tropospheric burdens of OH, ozone, and NO_x, Geophys. Res. Lett., 32, L16809, doi:10.1029/2005GL023419, 2005.

Liang, X. Z., Kunkel, K. E., and Samel, A. N.: Development of a regional climate model for US Midwest applications. Part I: Sensitivity to buffer zone treatment, J. Clim., 14, 4363–4378, 2001.

Liebl, K. H. and Seiler, W.: CO and H_2 destruction at the soil surface, Microbial Production and Utilization of Gases, edited by: Schlegel, H. G., Gottschalk, G., and Pfenning, N., Goltze, Göttingen, Germany, 215–229, 1976.

Lin, J. T., Patten, K. O., Hayhoe, K., Liang, X. Z., and Wuebbles, D. J.: Effects of future climate and biogenic emissions changes on surface ozone over the United States and China, J. Appl. Meteorol. Clim., 47, 1888–1909, 2008a.

Lin, J., Wuebbles, D. J., and Liang, X.: Effects of intercontinental transport on surface ozone over the United States: Present and future assessment with a global model, Geophys. Res. Lett., 35, L02805, doi:10.1029/2007GL031415, 2008b.

Luecken, D. J., Phillips, S., Sarwar, G., and Jang, C.: Effects of using the CB05 vs. SAPRC99 vs. CB4 chemical mechanism on model predictions: Ozone and gas-phase photochemical precursor concentrations, Atmos. Environ., 42, 5805–5820, 2008.

Novelli, P. C., Lang, P. M., Masarie, K. A., Hurst, D. F., Myers, R., and Elkins, J. W.: Molecular hydrogen in the troposphere: Global distribution and budget, J. Geophys. Res., 104, 30427–30444, 1999.

Olivier J., Peters, J., Granier, C., Petron, G., Muller, J. F., and Wallens, S.: Present and future surface emissions of atmospheric compounds, POET report #2, EU project EVK2-1999-00011, 2003.

Pfister, G. G., Hess, P. G., Emmons, L. K., Rasch, P. J., and Vitt, F. M.: Impact of the summer 2004 Alaska fires on top of the atmosphere clear-sky radiation fluxes, J. Geophys. Res., 113, D02204, doi:10.1029/2007JD008797, 2008.

Prather, M. J.: An environmental experiment with H_2?, Science, 302, 581–582, 2003.

Price, H., Jaegle, L., Rice, A., Quay, P., Novelli, P. C., and Gammon, R.: Global budget of molecular hydrogen and its deuterium content: Constraints from ground station, cruise, and aircraft observations, J. Geophys. Res., 115, D12306, doi:10.1029/2009JD012529, 2007.

Sarwar, G., Luecken, D., Yarwood, G., Whitten, G. Z., and Carter, W. P. L.: Impact of an updated carbon bond mechanism on predictions from the CMAQ modeling system: Preliminary assessment, J. Appl. Meteorol. Clim., 47, 3–14, 2008.

Schultz, M. G., Diehl, T., Brasseur, G. P., and Zittel, W.: Air pollution and climate-forcing impacts of a global hydrogen economy, Science, 302, 624–627, 2003.

Seiler, W. and Zankl, H.: Die Spurengase CO und H_2 uber Munchen, Umschau, 75, 735–736, 1975.

Simmonds, P. G., Derwent, R. G., O'Doherty, S., Ryall, D. B., Steele, L. P., Langenfelds, R. L., Salameh, P., Wang, H. J., Dimmer, C. H., and Hudson, L. E.: Continuous high-frequency observations of hydrogen at the Mace Head baseline atmospheric monitoring station over the 1994–1998 period, J. Geophys. Res., 105, 12105–12121, 2000.

Smith-Downey, N. V., Randerson, J. T., and Eiler, J. M.: Molecular hydrogen uptake by soils in forest, desert, and marsh ecosystems in California, J. Geophys. Res., 113, G03037, doi:10.1029/2008JG000701, 2008.

Spivakovsky, C. M., Logan, J. A., Montzka, S. A., Balkanski, Y. J., Foreman-Fowler, M., Jones, D. B., Horowitz, L. W., Fusco, A. C., Brenninkmeijer, C. A. M., Prather, M. J., Wofsy, S. C., and McElroy, M. B.: Three-dimensional climatological distribution of tropospheric OH: Update and evaluation, J. Geophys. Res., 105, 8931–8980, doi:10.1029/1999JD901006, 2000.

Tie, X. X., Madronich, S., Walters, S., Edwards, D. P., Ginoux, P., Mahowald, N., Zhang, R. Y., Lou, C., and Brasseur, G.: Assessment of the global impact of aerosols on tropospheric oxidants, J. Geophys. Res., 110, D03204, doi:10.1029/2004JD005359, 2005.

Tromp, T. K., Shia, R. L., Allen, M., Eiler, J. M., and Yung, Y. L.: Potential environmental impact of a hydrogen economy on the stratosphere, Science, 300, 1740–1742, 2003.

United States Environmental Protection Agency (U.S. EPA): Air Emissions by Pollutant, available at: http://www.epa.gov/air/emissions/, 2009.

van der Werf, G. R., Randerson, J. T., Giglio, L., Collatz, G. J., Kasibhatla, P. S., and Arellano Jr., A. F.: Interannual variability in global biomass burning emissions from 1997 to 2004, Atmos. Chem. Phys., 6, 3423–3441, doi:10.5194/acp-6-3423-2006, 2006.

Vollmer, M. K., Juergens, N., Steinbacher, M., Reimann, S., Weilenmann, M., and Buchmann, B.: Road vehicle emissions of molecular hydrogen (H_2) from a tunnel study, Atmos. Environ., 41, 8355–8369, 2007.

Warwick, N. J., Bekki, S., Nisbet, E. G., and Pyle, J. A.: Impact of a hydrogen economy on the stratosphere and troposphere studied in a 2-D model, Geophys. Res. Lett., 31, L05107, doi:10.1029/2003GL019224, 2004.

World Health Organization/Europe (WHO/Europe): Health aspects of air pollution with particulate matter, ozone and nitrogen dioxide: Report on a WHO working group, Bonn, Germany, 2003.

Wu, S., Mickley, L. J., Jacob, D. J., Rind, D., and Streets, D. G.: Effects of 2000-2050 changes in climate and emissions on global tropospheric ozone and the policy-relevant background surface ozone in the United States, J. Geophys. Res., 113, D18312, doi:10.1029/2007JD009639, 2008.

Yonemura, S., Kawashima, S., and Tsuruta, H.: Continuous measurements of CO and H_2 deposition velocities onto an andisol: uptake control by soil moisture, Tellus B, 51, 688–700, 1999.

Yonemura, S., Kawashima, S., and Tsuruta, H.: Carbon monoxide, hydrogen, and methane uptake by soils in a temperate arable field and a forest, J. Geophys. Res., 105, 14347–14362, 2000.